Energy Conversion and Management 258 (2022) 115484

Contents lists available at ScienceDirect

Energy Conversion and Management

journal homepage: www.elsevier.com/locate/enconman

Thermo-economic assessment of flexible nuclear power plants in future low-carbon electricity systems: Role of thermal energy storage

Abdullah A. Al Kindi [a], Marko Aunedi [b], Antonio M. Pantaleo [a,c], Goran Strbac [b], Christos N. Markides [a,*]

[a] Clean Energy Processes (CEP) Laboratory, Department of Chemical Engineering, Imperial College London, London SW7 2AZ, United Kingdom
[b] Department of Electrical and Electronic Engineering, Imperial College London, London SW7 2AZ, United Kingdom
[c] Department of Agro-Environmental Sciences, University of Bari Aldo Moro, Bari 70121, Italy

ARTICLE INFO

Keywords:
Nuclear power
Power flexibility
Power system optimisation
Steam Rankine cycle
Steam turbines
Thermal energy storage

ABSTRACT

The increasing penetration of intermittent renewable power will require additional flexibility from conventional plants, in order to follow the fluctuating renewable output while guaranteeing security of energy supply. In this context, coupling nuclear reactors with thermal energy storage could ensure a more continuous and efficient operation of nuclear power plants, while at other times allowing their operation to become more flexible and cost-effective. This study proposes options for upgrading a 1610-MW_{el} nuclear power plant with the addition of a thermal energy storage system and secondary power generators. The total whole-system benefits of operating the proposed configuration are quantified for several scenarios in the context of the UK's national electricity system using a whole-system model that minimises the total system costs. The proposed configuration allows the plant to generate up to 2130 MW_{el} during peak load, representing an increase of 32% in nominal rated power. This 520 MW_{el} of additional power is generated by secondary steam Rankine cycle systems (i.e., with optimised cycle thermal efficiencies of 24% and 30%) and by utilising thermal energy storage tanks with a total heat storage capacity of 1950 MWh_{th}. Replacing conventional with flexible nuclear power plants is found to generate whole-system cost savings between £24.3m/yr and £88.9m/yr, with the highest benefit achieved when stored heat is fully discharged in 0.5 h. At an estimated cost of added flexibility of £42.7m/yr, the proposed flexibility upgrades to such nuclear power plants appears to be economically justified with net system benefits ranging from £4.0m/yr to £31.6m/yr for the examined low-carbon scenarios, provided that the number of flexible nuclear plants in the system is small. This suggests that the value of this technology is system dependent, and that system characteristics should be adequately considered when evaluating the benefits of different flexible nuclear plant configurations and choosing the most cost-effective designs and operational characteristics.

1. Introduction

Although recent rapid reductions in the cost of renewable generation technologies have been making nuclear power less economically attractive due to its high capital costs, long construction times, and uneconomic load-following operation, nuclear power can play a significant role in achieving the ambitious global emission reduction targets due to its ability to provide zero-carbon electricity [1]. In particular, nuclear power or other forms of firm low-carbon generation will be essential for ensuring energy security in a system with a high share of variable renewables. This is why the UK is still considering government-supported models for investing in nuclear power projects as part of the overall effort to achieve the objective of net-zero greenhouse emissions by 2050 under the Climate Change Act [2,3].

Nuclear power plants are commonly operated to meet baseload electricity demand because of their economic and technical characteristics. However, in systems with a high share of renewables it is important to investigate how flexible and profitable nuclear power can complement renewables, not only by meeting baseload demand but also by supplying peak demand. Jenkins et al. [4] investigated the benefits of nuclear flexibility in power system operation with a high penetration of wind and solar. The study concluded that flexible nuclear operation potentially reduces the operating costs and increases the overall reactor revenues by 2–5% compared to a baseload nuclear reactor. The increase of revenues is mainly due to the capability of supplying day-ahead

* Corresponding author.
E-mail address: c.markides@imperial.ac.uk (C.N. Markides).

https://doi.org/10.1016/j.enconman.2022.115484

Available online 24 March 2022

Nomenclature

Symbols

C	operating cost function (£)
E	number of electrolyser assets (-)
G	number of power generation assets (-)
h	specific enthalpy (J/kg)
H	number of hydrogen storage assets (-)
$\dot{m}$	mass flowrate (kg/s)
n	number (-)
N	number of flexible nuclear assets (-)
Q	heat (J)
$\dot{Q}$	rate of heat (W)
S	number of battery storage assets (-)
t	time interval (h)
T	temperature (K)
u	unit commitment (-)
$\dot{W}$	power (W)
x	steam quality (-)

Greek symbols

α	availability factor (-)
β	no-load heat rate (MWh_{th}/h)
γ	incremental heat rate (MW_{th}/MW_{el})
δ	duration of unit time interval (h)
Δ	difference (-)
η	efficiency (%)
μ	total capacity (W)
π	per-unit cost (£/W/yr)
τ	number of time intervals (h)

Subscripts/superscripts

Ch	charging
D	design point
Dch	discharging
DE	deaerator
FN	flexible nuclear
Gen	generator
HL	hot-leg
HPT	high-pressure turbine
in	inlet
is	isentropic
LPT	low-pressure turbine
m	melting
max	maximum
min	minimum
net	net
OD	off-design point
out	outlet
P	pump
PL	part-load
pp	pinch-point
PSRC	primary steam Rankine cycle
RH	reheater
SE	side extraction
SG	steam generator
SSRC	secondary steam Rankine cycle
T	turbine
TES	thermal energy storage
TV	throttling valve

Acronyms

AGR	advanced gas-cooled reactor
BECCS	bioenergy with carbon capture and storage
BESS	battery energy storage system
CCGT	combined cycle gas turbine
CCS	carbon capture and storage
CFWH	closed feedwater heater
CHP	combined heat and power
CSP	concentrated solar power
DSR	demand side response
EPR	European pressurised reactor
HPT	high-pressure turbine
IRENA	international renewable energy agency
LAES	liquid air energy storge system
LCOE	levelised cost of electricity
LPT	low-pressure turbine
LWR	light water reactor
OCGT	open cycle gas turbine
OPEX	operating expenditure
ORC	organic Rankine cycle
PCM	phase change material
PSRC	primary steam Rankine cycle
PV	photovoltaic
PWR	pressurised water reactor
RH	reheater
SG	steam generator
SSRC	secondary steam Rankine cycle
TES	thermal energy storage
WeSIM	whole-electricity system investment model

reserves and avoiding negative day-ahead electricity prices. Furthermore, a study performed by Denholm et al. [5] conceptually studied the impact of integrating thermal energy storage (TES) system with nuclear power plants. The study recommended the use of TES systems to achieve higher capacity factors and lower levelised cost of electricity (LCOE), especially where nuclear is competing with intermittent renewables.

Combining nuclear reactors with TES systems for enhanced flexibility and increased revenues has been previously investigated in the literature. For example, Carlson et al. [6] investigated the impact of integrating a pressurised water reactor (PWR), Westinghouse AP1000, with TES tanks. The TES tanks are charged by diverting excess steam after the steam generator during low demand and are discharged to the main nuclear-powered Rankine cycle system that includes turbines that can be operated at about 10% higher power output than the design point. Several TES materials such as concrete, silica and phase change material (PCM) were considered. It was concluded that such integration could potentially increase the capacity factor by up to 10% compared to operating the same power plant with steam bypass option. Park et al. [7] performed a technoeconomic study on integrating a nuclear power plant with liquid air energy storage system (LAES). In that study, charging is performed by diverting steam from the nuclear-powered cycle to drive an external steam turbine driven compressor utilised for air compression in the LAES, while discharging is performed similar to conventional LAES systems. This nuclear-LAES integrated system resulted in increasing the capacity factor for the nuclear power plant by 3% and decreasing the LCOE of the LAES from 220 $/MWh_{el}$ (i.e., for standalone LAES) to 183 $/MWh_{el}$. Furthermore, Amuda et al. [8] explored the option of combining a currently operating light water reactor (LWR) plant (APR1400) with packed-beds (i.e., crushed rocks) TES system. In the proposed configuration, which was selected based on an optimisation and exergy study performed by Kluba et al. [9], the TES is utilised to provide extra feedwater heating in the primary power generation cycle,

which results in 135 MW_{el} of additional electrical power when the reactor is operated at full thermal capacity. This additional power can be supplied to the electricity grid during high demand to increase revenues. Other TES systems including molten-salt tanks [10], firebrick resistance-heated energy system [11], geothermal heat storage [12], cryogenic air energy storage [13] and hot rock storage [14] were also considered and discussed.

There are also several studies that considered the option of coupling nuclear reactors not only with TES systems but also with secondary power generators for extra peak power generation. Carlson et al. [15] conducted a thermodynamic analysis of coupling the AP1000 reactor with a TES system and secondary power generation cycle (steam Rankine cycle). Four different configurations were considered based on the location of the TES system (i.e., where steam is diverted for charging stream) and whether stored thermal energy is discharged using the primary or the secondary power generation cycle. It was found that the option where TES tanks are charged by heat from steam diverted after the moisture separator/reheater and then discharged using the optimised secondary power generation cycle gives the greatest thermodynamic performance compared to the other considered options. This charge/discharge option resulted in increasing the capacity factor of AP1000 by 15% compared to the bypass option that is generally used for baseload flexibility. Carlson et al. [16] also performed a parametric study investigating the thermodynamics and the cost performance of coupling the same reactor with a TES system and a secondary Rankine cycle system. Three configurations based on the TES charge/discharge mechanisms and duration were investigated, and two of these configurations could provide more than 1.5 times the nominal power output of 1050 MW_{el} due to the use of secondary power generators. Moreover, the integration of nuclear power plant with a cryogenic-based energy storage technology and secondary power generation unit was assessed by Li et al. [17]. The studied configuration showed the ability of generating a total net output power of 690 MW_{el} during peak times, which is 2.7 times the baseload power output of 250 MW_{el}.

In terms of economics, Forsberg [18] investigated the potential economic benefits of integrating LWRs with heat storage and auxiliary fuel combustion heater. The combustion heater was added to assure a continuous peak electricity production, even when the stored heat in the TES system is fully depleted. It was concluded that the economics of this combination is dependent on three conditions: (i) the cost of heat storage is lower than the cost of electricity storage technologies, (ii) the cost of the nuclear reactor and the steam generators is higher than the costs of power generation cycle components, and (iii) low-cost boilers should provide assured peak-load capacity at lower costs than competing technologies such as combined cycle gas turbines (CCGTs). Romanos et al. [19] investigated the thermodynamics and the economic feasibility of upgrading the flexibility of the UK's current fleet of advanced gas-cooled reactors (AGRs) through the integration with PCM-based TES system and secondary organic Rankine cycle (ORC) generators. The study found that such integration could increase the peak power output from 670 MW_{el} to 822 MW_{el} (i.e., 24% increase) during the discharge of thermal energy from the PCM tanks. The study concluded that the economics of the upgraded AGRs is highly dependent on: (i) the difference between off-peak and peak electricity prices; (ii) the size of the ORC plants; and (iii) the frequency and the duration of the charging/discharging cycles. Another study performed by Borowiec et al. [20] focused on the potential economic benefits of running a 3.5 GW_{th} nuclear reactor coupled with a TES system in five different electricity markets in the USA. The study considered various market scenarios based on the shares of renewables (i.e., wind and solar) and several capacity prices. It was concluded that profitability could be attained but it is highly dependent on: (i) the type of electricity markets; (ii) the share of renewables in the system; (iii) the size of installed capacity of nuclear and renewables; and (iv) the installation costs and the storage materials of the attached TES system. All aforementioned research demonstrated the potential of flexible and profitable nuclear operation with the integration of TES, while keeping the reactor output at full rated power. However, the gained benefits, from electricity systems perspective, of replacing conventional nuclear power plants with enhanced flexibility ones has not been thoroughly studied and quantified yet.

There is a wide range of TES technologies, which can be classified in terms of storage mechanism as: i) sensible, ii) latent, also known as PCM, and iii) thermochemical [21]. There is a growing demand for TES, as reported in a recent study by the International Renewable Energy Agency (IRENA) [22] that predicts that the global market for TES could triple in size by 2030, with an increase from 234 GWh_{th} of installed capacity in 2019 to over 800 GWh_{th} within a decade. Recent research from Cardenas et al. [23] estimated the required heat storage capacity as the penetration of renewables increases, and the timescales in which energy is most efficiently stored. The paper studied the effect that the renewable penetration, allowable curtailment, storage capacity and efficiency have on the total cost of electricity in the UK scenario, concluding that the most needed flexibility service at high solar photovoltaic (PV) and wind energy penetration is the medium duration one, with 4 to 200 h discharge duration.

The role of TES in systems with high renewable penetrations becomes even more prominent when considering renewable technologies such as concentrated solar power (CSP). This is evident in Gils et al. [24] paper, which analyses different European scenarios with very high renewable penetrations and discusses the economic and technical issues. The advantages of the application of TES over batteries in combination with large-scale thermoelectric power plants were also highlighted by Ma et al. [25]. According to that analysis, the use of TES in combination with conventional power plants allows to economically support variable renewables at larger capacity and for longer discharging hours than current battery storage technologies or hydropower storage.

Decarbonisation of the electricity system will require a range of technologies to provide flexibility in the context of grid support, balancing, security of supply and integration of variable renewables [26]. These technologies will include various forms of energy storage, demand-side response, expansion of interconnection capacity and more flexible generation technologies, as well as a number of cross-vector flexibility options such as TES and power-to-X. A number of studies have shown that flexibility becomes increasingly important as carbon emissions targets for the electricity sector are reduced and therefore the provision of flexibility will become particularly critical in achieving net-zero carbon or net-negative carbon electricity supply [27].

Energy technologies linking heat and power will play a key role in the integration between the heating/cooling and electricity networks, and therefore recent research has focused on the optimal design and operation of combined heat and power (CHP) systems, centralised heat pumps and TES options for district heating [28]. It has been shown in Ref. [29] that a cost-efficient supply of heat in a local district heating system may require a significantly higher volume of TES to manage local grid constraints and support the integration of high penetration of variable renewables.

To adequately quantify the role of flexible solutions in future electricity systems, it is critical to model these systems with sufficient spatial-temporal resolution using a holistic system approach. The approach to system valuation of flexible nuclear configurations used in this paper is based on an extension of the whole-system modelling approach presented in Ref. [30]. This whole-system valuation approach has previously been used to assess battery storage [31], pumped-hydro storage [32] and liquid-air and pumped-heat energy storage [33].

In this paper, a novel approach to configuring flexible nuclear power plants and quantifying their system value in low-carbon electricity systems is proposed. Specifically, the main novel contributions of the paper include:

- A technology-rich approach to configuring the design of a selected flexible nuclear power station and simulating its operation based on detailed thermodynamic modelling of various individual plant

components (secondary Rankine power cycle systems, generators, turbines, PCM-based TES tanks, feed pumps, condensers, feedwater heaters, etc.), including the consideration of part-load operation conditions during the charge cycle of the TES system.
- The design of novel modular units combining PCM-based TES systems and secondary steam Rankine cycle power systems, aiming for a more feasible installation procedure and potentially lower costs of the main components of such an integrated system.
- Optimisation of the thermodynamic performance of the proposed flexible nuclear plant configuration by determining efficient choices for a variety of technical parameters including the choice of suitable PCMs.
- Development of a high-fidelity model of the resulting flexible nuclear power plant within a high-resolution power system model that minimises the total investment and operation cost for generation and storage assets in the system; representation of flexible nuclear includes an explicit consideration of different plant components including TES, steam generator and primary and secondary generation cycles.
- Quantification of the system value offered by the enhanced flexibility of such nuclear plants, considering a range of scenarios characterised by decarbonised electricity supply and a high share of variable renewable generation.

2. Methods

As a first step of this study, a layout is proposed for upgrading a conventional nuclear power plant with a TES system and secondary power generation systems. Each main component of the proposed configuration is computationally modelled for thermodynamic performance evaluation. Secondly, the obtained energy performance and investment costs are used as an input for the whole-system modelling of the low-carbon electricity system in the UK, to evaluate the benefits of such a flexible asset.

2.1. Power plant configuration and description

The layout of the proposed nuclear power plant, illustrated in Fig. 1, consists of:

1) A nuclear power island that includes a PWR and a steam generator (SG), which generates steam utilising nuclear thermal power.
2) A primary steam Rankine cycle (PSRC) system that contains high-pressure turbines (HPT), low-pressure turbines (LPT), a reheater (RH), a condenser, electric generators, six closed feedwater heaters (CFWH), throttling valves, control valves, a condensate pump, a feed pump and a deaerator.
3) TES units, indicated as TES-1 and TES-2 in Fig. 1. TES-1 unit is proposed to have two PCM tanks (PCM-1 and PCM-2) connected in series. PCM-1 tank is charged using higher temperature steam flowing out from the steam generator, while PCM-2 tank is charged using steam flowing out from PCM-1 tank. Similarly, TES-2 unit has two PCM tanks (PCM-3 and PCM-4), also connected in series. However, TES-2 tanks are charged by lower temperature steam that is extracted after the HPT and before the reheater, as shown in Fig. 1.
4) Two secondary steam Rankine cycle (SSRC-1 and SSRC-2) systems. System SSRC-1 is operated by discharging the heat stored in TES-1 tanks while system SSRC-2 is operated by utilising the stored heat in TES-2 tanks.

In this study, the reactor is assumed to continuously operate at full rated thermal power whenever it is possible in order to avoid power disturbance in the reactor and to maximise the economic benefits of investing in such a capital-intensive energy source. In this context, most

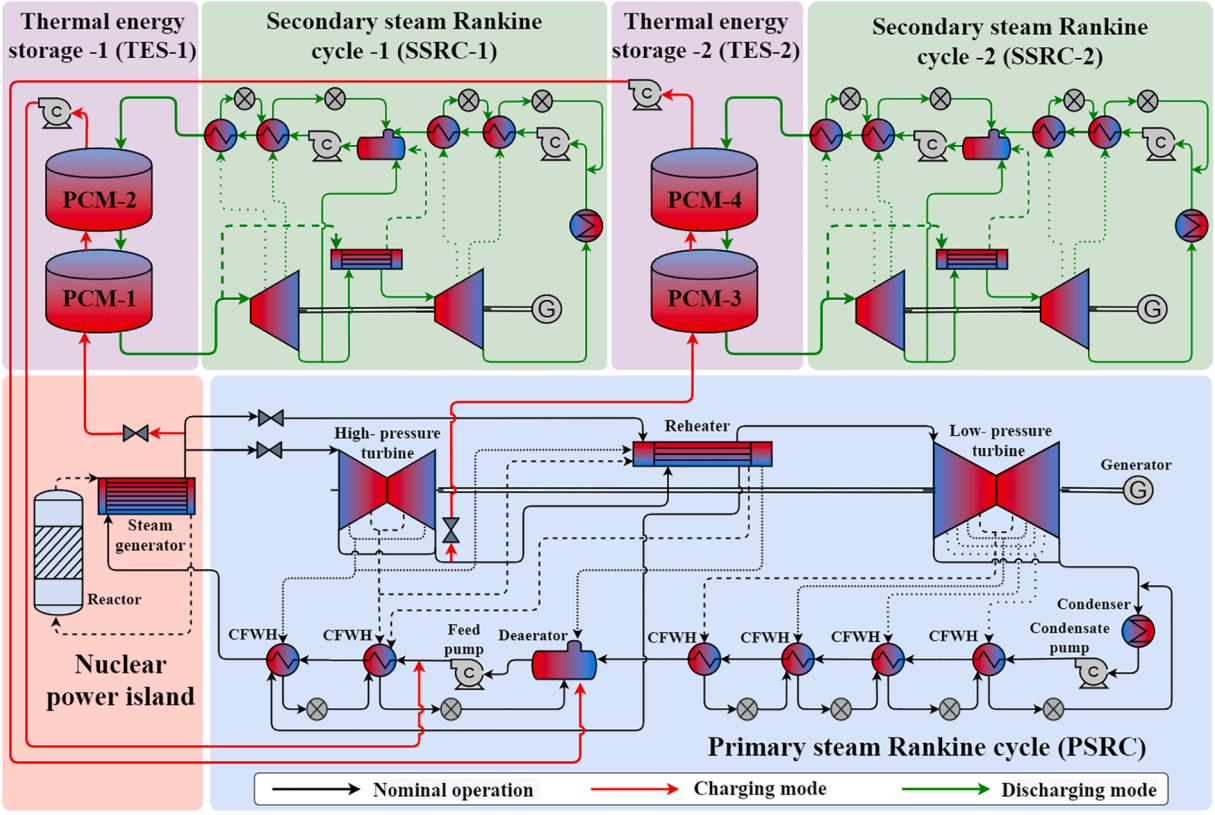

Fig. 1. Layout of the proposed nuclear power plant coupled with PCM tanks as TES units and secondary power Rankine cycle (SSRC) systems. Black lines indicate flow streams during nominal operation, red lines indicate thermal energy charging flow streams, and green lines indicate thermal energy discharging flow streams. (For interpretation of the references to colour in this figure legend, the reader is referred to the web version of this article.)

load following operations are achieved by controlling: (i) the amount of steam flowing from the steam generator to the PSRC system; (ii) the amount of steam directed to both TES units (i.e., charging mode); and (iii) the operation of both SSRC systems (i.e., discharging mode).

During nominal (full load) operation mode, the generated steam in the SG flows to the PSRC system and no steam is directed to the TES units as the TES system control valves (i.e., located before PCM-1 and PCM-3 tanks) are closed. The TES system charging process is performed at times of low electricity demand (i.e., part-load operation mode) by opening the TES system valves and allowing some amount of the generated steam to flow into the PCM tanks for heat deposition. The opening of TES valves reduces the mass flowrate of steam flowing to the PSRC system (i.e., to the HPT, reheater and LPT) due to constant steam generation in the SG. This operation method allows for operating the PSRC system at reduced power output while running the reactor at full rated thermal power output (i.e., steady steam outlet conditions from the SG). The stored heat in the TES system is assumed to be discharged to generate extra electrical power through the operation of the SSRC systems during periods of high demand (i.e., peak electricity prices). The use of SSRC systems is to have the ability to generate extra power during high electricity prices, and thus, higher revenues.

2.2. Nuclear reactor and primary steam Rankine cycle system

The selected nuclear reactor design is the European pressurised reactor (EPR), which is a PWR that generates 4520 MW_{th} of thermal power using nuclear fission [34]. Although there is a wide range of reactor types and designs, the EPR is chosen as it is currently under construction in the UK at Hinkley Point C, and is also the choice for the potential future construction of Sizewell C [35]. It is expected that the EPR design has a higher potential than other reactor designs to replace the current fleet of AGRs in the UK due to the experience gained from constructing current EPRs. Table 1 summarises the main EPR operating parameters that are considered in the PSRC system model, which is explained in detail in the next section.

2.2.1. Full load operation

The full load (nominal load) of the PSRC system model is formulated using the operation parameters and assumptions listed in Table 2. Full load operation of the PSRC system means that no steam is directed to the TES units and all nuclear thermal power is utilised for electrical power generation from the PSRC generators. The enthalpy of steam exiting the nuclear-powered SG is calculated using the rate of added heat in the steam generator, $\dot{Q}_{SG}$, as follows:

$$\dot{Q}_{SG} = \dot{m}\ (h_{out} - h_{in}) \tag{1}$$

where $\dot{Q}_{SG}$ is the (rate of) added heat, $\dot{m}$ the mass flowrate, h the specific enthalpy of steam, and subscripts 'in' and 'out' indicate the conditions at the inlet and the outlet of the steam generator.

Equations (2)-(5) are used to calculate the generated power by the turbines and needed by the pumps:

$$\dot{W}_T = \dot{m}\ (h_{in} - h_{out}) \tag{2}$$

Table 1
Main operation parameters of the EPR.

Parameter	Value	Reference
Reactor thermal power (MW_{th})	4520	[34]
Feedwater temperature (°C)	230	[36]
Feedwater pressure (kPa)	8300	[37]
Steam generator mass flowrate (kg/s)	2553	[36]
Steam generator outlet temperature (°C)	293	[37]
Steam generator outlet pressure (kPa)	7800	[37]

Table 2
Primary steam Rankine cycle assumptions and parameters at nominal power.

Parameter	Value	Reference
Average HPT design isentropic efficiency (%)	87	[38]
Average LPT design isentropic efficiency (%)	87	[38]
Condensing pressure (kPa)	10	[16]
Pump isentropic efficiency (%)	85	[38]
Generator mechanical efficiency (%)	98	[39]
Pressure loss in the reheater (kPa)	300	–
Hot stream outlet steam quality in CFWHs (-)	0	–

$$\eta_T = \frac{(h_{in} - h_{out})}{(h_{in} - h_{out,is})} \tag{3}$$

$$\dot{W}_P = \dot{m}\ (h_{out} - h_{in}) \tag{4}$$

$$\eta_P = \frac{(h_{out,is} - h_{in})}{(h_{out} - h_{in})} \tag{5}$$

where $\dot{W}_T$ and η_T are the turbine power and isentropic efficiency, $\dot{W}_P$ and η_P the pump power and isentropic efficiency, and subscript 'is' indicates properties evaluated at equivalent isentropic conditions.

The amount of thermal power added in all CFWHs and the reheater and the outlet steam enthalpy of the deaerator are calculated using Equations (6) and (7), respectively:

$$\dot{Q}_{CFWH,RH} = \dot{m}\ (h_{out} - h_{in}) \tag{6}$$

$$h_{out} = \frac{\sum (\dot{m}h)_{in}}{\sum \dot{m}_{in}} \tag{7}$$

where $\sum (\dot{m}h)_{in}$ is the sum of all inlet flow energy and $\sum \dot{m}_{in}$ the sum of inlet mass flowrates.

The PSRC system net electrical power, $\dot{W}_{net}$, and the net PSRC system efficiency, η_{PSRC}, are calculated from:

$$\dot{W}_{net} = \left(\eta_{Gen} \sum \dot{W}_T\right) - \sum \dot{W}_P \tag{8}$$

$$\eta_{PSRC} = \frac{\dot{W}_{net}}{\dot{Q}_{SG}} \tag{9}$$

where η_{Gen} is the generator efficiency.

One method of obtaining the operating conditions of other PSRC system parameters such as the turbine side extraction pressures and flowrates, steam that flows from the steam generator to the reheater, etc., is to set up an optimisation model with an objective function that maximises the net cycle efficiency as in Equation (10). The model simulations are performed using MATLAB and all steam properties are obtained using REFPROP [40]. The PSRC system efficiency optimisation tasks are solved using MATLAB's interior point algorithm *fmincon*. This algorithm identifies multiple local minima over a range of initial conditions in order to find the global minimum.

$$\max_{\dot{m}_{RH(1,2,3)}, P_{HPT,SE(1,2)}, P_{HPT,out}, P_{LPT,SE(1,2,3,4)}, \dot{m}_{HPT,SE(1,2)}, \dot{m}_{LPT,SE(1,2,3,4)}} \{\eta_{PSRC}\} \tag{10}$$

where η_{PSRC} is the PSRC efficiency, $\dot{m}_{RH(1,2,3)}$ the mass flowrates of steam flowing to the reheater, $P_{HPT,SE(1,2)}$ the HPT side extractions pressures, $P_{HPT,out}$ the HPT main outlet pressure, $P_{LPT,SE(1,2,3,4)}$ the LPT side extractions pressures, $\dot{m}_{HPT,SE(1,2)}$ the steam mass flowrates from the HPT side extractions to high-pressure CFWHs, and $\dot{m}_{LPT,SE(1,2,3,4)}$ the steam mass flowrates from the LPT side extractions to low-pressure CFWHs.

The objective function is formulated to solve the numerical PSRC system model while satisfying a set of non-linear constraints listed in Equations (11)-(16):

$$\Delta T^{PP}_{CFWH,in} \geq 5\ ^{\circ}C \tag{11}$$

$$\Delta T^{PP}_{CFWH,out} \geq 5\ ^{\circ}C \tag{12}$$

$$x^{HL}_{CFWH,out} \leq 0 \tag{13}$$

$$P_{TV,out} = P^{HL}_{CFWH,in} \tag{14}$$

$$x_{P,in} \leq 0 \tag{15}$$

$$T_{RH,out} \geq 287^{\circ}C \tag{16}$$

where $\Delta T^{PP}_{CFWH,in}$ and $\Delta T^{PP}_{CFWH,out}$ are the inlet and outlet pinch-point temperature difference of all CFWHs, $x^{HL}_{CFWH,out}$ the CFWH hot-leg outlet steam quality, $P_{TV,out}$ the throttling valve outlet pressure, $P^{HL}_{CFWH,in}$ the CFWH hot-leg inlet steam pressure, $x_{P,in}$ the pump inlet steam quality, and $T_{RH,out}$ the reheater outlet temperature.

The constraints related to the pinch-point temperature differences in the CFWHs are set to allow for more effective heat transfer rates between the hot and the cold streams during nominal and part-load operation modes while achieving reasonable sizes (i.e., costs) of heat exchangers. The CFWH hot-leg outlet steam quality constraint, Equation (13), is to maximise the amount of heat transferred from the turbine side extraction steam to the feedwater through a full condensation of steam, leading to higher cycle thermal efficiencies. The pressure equality constraint, Equation (14), is to ensure that both CFWH inlets (i.e., from the turbine side extraction and from the throttling valve) have the same pressure. The pump inlet steam quality constraint is necessary to ensure that the steam entering the pumps is either saturated or subcooled liquid to avoid damaging the pumps. Lastly, the reheater steam temperature constraint is implemented to achieve higher cycle thermal efficiencies.

2.2.2. Part-load operation (charging mode)

The part-load PSRC system model is constructed by considering the following off-design turbine efficiency correlation for both, the HPT and the LPT [41]:

$$\eta^{OD}_{T} = \eta^{D}_{T} - 2\left(\frac{N^{OD}\sqrt{\Delta h^{D}_{is}}}{N^{D}\sqrt{\Delta h^{OD}_{is}}} - 1\right)^{2} \tag{17}$$

where η_T is the turbine isentropic efficiency, N the shaft rotational speed, Δh_{is} the equivalent isentropic enthalpy change across the turbine stage, and superscripts 'D' and 'OD' indicate the design point and off-design conditions, respectively.

It is assumed that the shaft speed is constant for all loads as the shaft is connected to a power grid with fixed frequency, typically 50 Hz in the UK [42]. In this study, the multiple stages between the turbine inlet and the next side extraction, between two side extractions or between the last side extraction and the main turbine outlet, are considered as one turbine stage. Therefore, the HPT turbine and the LPT are assumed to consist of 3 and 5 stages, respectively.

The part-load PSRC system model also considers the change of steam pressure at the inlet and the outlet of each stage due to steam mass flowrate and temperature variations inside the turbine during part-load operation. To calculate the turbine inlet, outlet, and side extractions pressure, the following Stodola's ellipse law is applied [43,44]:

$$\frac{\frac{\dot{m}^{OD}_{in}\sqrt{T^{OD}_{in}}}{P^{OD}_{in}}}{\frac{\dot{m}^{D}_{in}\sqrt{T^{D}_{in}}}{P^{D}_{in}}} = \frac{\sqrt{1-\left(\frac{P^{OD}_{out}}{P^{OD}_{in}}\right)^{2}}}{\sqrt{1-\left(\frac{P^{D}_{out}}{P^{D}_{in}}\right)^{2}}} \tag{18}$$

where P_{in} is the inlet steam pressure, P_{out} the outlet steam pressure, T_{in} the inlet steam temperature, and $\dot{m}_{in}$ the inlet steam mass flowrate.

The part-load cycle efficiency expression and the adjusted optimisation objective function are:

$$\eta^{PL}_{PSRC} = \frac{\dot{W}_{net}}{\dot{Q}_{SG} - \dot{Q}_{TES}} \tag{19}$$

$$\max_{\dot{m}_{RH(1,2,3)}, \dot{m}_{HPT,SE(1,2)}, \dot{m}_{LPT,SE(1,2,3,4)}, \dot{m}_{TES-1}, \dot{m}_{TES-2}} \{\eta^{PL}_{PSRC}\} \tag{20}$$

where $\dot{Q}_{TES}$ is the total amount of thermal power available for storage, $\dot{m}_{TES-1}$ the steam mass flowrate flowing to TES-1, and $\dot{m}_{TES-2}$ the steam mass flowrate directed to TES-2.

The optimisation problem is solved using the same optimisation algorithm as in Section 2.2.1 and satisfying the constraints listed in Equations (11)-(16) as well as the following additional constraint that is set to limit the amount of diverted steam from the PSRC system (i.e., before and after the HPT) to the TES system during the charging mode, which reduces the overall impact on the performance of both turbines during off-design conditions:

$$\dot{Q}_{TES-1} = \dot{Q}_{TES-2} \tag{21}$$

where $\dot{Q}_{TES-1}$ and $\dot{Q}_{TES-2}$ are the amount of thermal power available for storage in TES-1 (PCM-1 and PCM-2 tanks) and in TES-2 (PCM-3 and PCM-4 tanks), respectively.

It should be noted that the SG inlet temperature is assumed to be maintained at 230 °C during the charging process of the TES systems. The temperature of steam exiting PCM-2 and PCM-4 tanks is expected to vary during the TES charging process, but these temperature variations are controlled in the feedwater heating system (i.e., the CFWHs and the deaerator). This can be seen in Fig. 1 where steam outflowing from the TES-1 system is directed to the cold-leg inlet of the first high-pressure CFWH and steam exiting the TES-2 system is connected to the deaerator, which also operates as an open feedwater heater. The temperature control in the feedwater heating system is achieved by adjusting the amount (i.e., the mass flowrate) of steam flowing from the turbine side extractions. This affects the amount of heat transferred to the feedwater in the CFWHs, and thus the feedwater temperature.

2.3. Conceptual design of modular thermal energy storage and secondary steam Rankine cycle units

A conceptual modular TES-SSRC design is proposed in this study. The modular TES-SSRC unit is designed to contain four components attached to the PSRC system. These components are system TES-1 (PCM-1 and PCM-2 tanks), system SSRC-1, system TES-2 (PCM-3 and PCM-4 tanks), and system SSRC-2 as illustrated in the top side of Fig. 1. The reasons behind proposing modular TES-SSRC units are:

- The potential of capital cost and production time reduction when fabricating the same component for multiple times (i.e., mass production) [45].
- The ability of adding extra modules if larger heat storage capacity is required in the future.
- The capability of placing the modular units in different locations around the nuclear reactor.

The size of the modular TES-SSRC unit is determined by the amount of thermal power available for storage and the TES charging/discharging duration. One modular TES-SSRC unit is sized based on the following assumptions:

- The storage capacities of TES-1 and TES-2 are determined by calculating the amount of heat available for storage when the PSRC power output is reduced by a scale of 10% of the nominal load for 1 h. For example, if the PSRC system is operating at 50% of its nominal

Table 3
Thermal properties of PCM and steam conditions of the PCM tanks.

Parameters		TES-SSRC-1		TES-SSRC-2	
		PCM-1 [48,51–54]	PCM-2 [49,50,53–57]	PCM-3 [50,58,59]	PCM-4 [49,50,53–57]
Material		$NaNO_2$	53% KNO_3 + 40% $NaNO_2$ + 7% $NaNO_3$	87% $LiNO_3$ + 13% NaCl	53% KNO_3 + 40% $NaNO_2$ + 7% $NaNO_3$
Melting temperature (°C)		282	142	208	142
Latent heat of fusion (kJ/kg)		212	81.5	369	81.5
Density (kg/m^3)		2020, 1810*	2000, 1960*	2350, 1890*	2000, 1960*
Specific heat capacity (kJ/kg·K)		1.85, 1.60*	1.34, 1.56*	1.54, 1.56*	1.34, 1.56*
Thermal conductivity (W/m·K)		1.30, 0.50*	0.57, 0.42*	1.35, 0.63*	0.57, 0.42*
Charging steam inlet condition	Pressure (kPa)	7800	–	2390	–
	Temperature (°C)	293	–	221	–
	Quality (-)	superheated	–	0.88	–
	Mass flowrate (kg/s)	102	102	111	111
Charging steam outlet conditions	Pressure (kPa)	–	7700	–	2290
	Temperature (°C)	–	152	–	152
	Quality (-)	–	subcooled	–	subcooled
	Mass flowrate (kg/s)	102	102	111	111

* First value is for the solid and the second for the liquid phase.

power for 1 h, 5 modular TES units can be fully charged at the end of that hour.

- Both systems (SSRC-1 and SSRC-2) are sized to fully discharge TES-1 and TES-2 in 1 h, which is selected based on the assumption of running the whole-electricity system optimisation model with 1-h time resolution (see Section 2.4 for more details).

2.3.1. Thermal energy storage system design and selection of phase change materials

PCMs are selected due to their ability to charge and discharge thermal power at constant temperatures (melting temperature) [46]. The optimal type and design (i.e., shape, dimensions, etc.) of the PCM tanks in the modular TES-SSRC system is not the focus of this study. However, the selection of the PCM type is essential to determine the operation temperature range of SSRC-1 and SSRC-2 systems. Table 3 summarises the calculated inlet steam conditions and the assumed outlet steam conditions of TES-1 and TES-2 as well as the types of PCM that suit the temperature range of the charging steam (heat-source). Each PCM tank is designed with a specific material, depending on the charging steam temperature and the correspondent PCM melting temperature, to reduce, to some extent, the exergy losses caused by large temperature differences between the PCM and the steam in the charging/discharging processes [19]. It should be emphasised that the size (i.e., volume) of the PCM tanks is expected to between 3000 m^3 and 3500 m^3 for each tank (i.e., calculated based on heat storage density of 46 kWh_{th}/m^3 as in Ref. [19]). Thus, sufficient land areas and spaces are required for the installation of these PCM tanks.

Selection of the PCM type is based on a minimum of 10 °C temperature difference between the melting temperature of the PCM and the inlet/outlet steam condition in order to ensure effective heat transfer rates between the flowing steam and the PCM. There are various types of PCMs such as: organic compounds (paraffin and non-paraffin compounds), inorganic compounds (salts, salt hydrate, and metallic), and eutectic which is a mixture of the previous types [47]. For a temperature range from 150 °C to 300 °C, salts and eutectic salts are good candidates because their melting temperature are within the specified range and also because their thermal conductivities (i.e., between 0.4 and 1.5 W/m·K) are relatively higher than those of most organic latent-heat storage materials, which could be as low as 0.1 W/m·K [48]. Therefore, $NaNO_2$ is selected for PCM-1 tank (melting temperature of 282 °C, which is 11 °C below the steam inlet temperature, 293 °C) [48]. For PCM-2 tank, the selected material is salt mixture referred to as HITEC (composition: 53 wt% KNO_3 + 40 wt% $NaNO_2$ + 7 wt% $NaNO_3$) with a melting point of 142 °C, which is 10 °C below the minimum steam temperature in TES-1 [49]. In TES-2, the selected PCM for tank 3 is an eutectic salt that comprises of 87 wt% $LiNO_3$ + 13 wt% NaCl, with a melting temperature of 208 °C, since the maximum steam temperature is 221 °C, which is lower than the maximum steam temperature in TES-2 [50]. For PCM-4 tank, the selected material is the same as in PCM-2 tank (i.e., HITEC).

It is also conservatively assumed that there is a pressure loss amounting to 50 kPa on the steam flow across each PCM tank, to account for any frictional losses in the tank during charging and discharging process. The mass flowrate listed in Table 3 is the average mass flowrate calculated when the PSRC power level is reduced in steps of 10% of nominal power, e.g., from 100% to 90%, from 90% to 80%, etc.

2.3.2. Design and operation of secondary steam Rankine cycle systems (discharging mode)

Discharging of stored heat is performed through system SSRC-1 and system SSRC-2 that are coupled to TES-1 and TES-2, respectively. The temperature range of TES-2 is relatively low for steam Rankine cycles, which might not be a favourable option. However, it is still considered in this study since the size of the SSRC systems is expected to be greater than 45 MW_{el}. Similarly, as in the PSRC efficiency optimisation model, the main steam parameters of the SSRCs are optimised with a set of non-

linear constraints to achieve maximum cycle efficiency. The optimisation objective function of each SSRC is as follows:

$$\max_{P_{\mathrm{TES,in}}, \dot{m}_{\mathrm{RH}}, P_{\mathrm{HPT,SE(1,2)}}, P_{\mathrm{HPT,out}}, P_{\mathrm{LPT,SE(1,2)}}, \dot{m}_{\mathrm{HPT,SE(1,2)}}, \dot{m}_{\mathrm{DE}}, \dot{m}_{\mathrm{LPT,SE(1,2)}}} \{\eta_{\mathrm{SSRC}}\} \tag{22}$$

where η_{SSRC} is the SSRC efficiency, $P_{\mathrm{TES,in}}$ the TES inlet pressure, $\dot{m}_{\mathrm{RH}}$ the steam mass flowrate directed to the reheater, $\dot{m}_{\mathrm{DE}}$ the mass flowrate directed to the deaerator, and the other parameters are as defined in Equation (10).

In addition to the constraints listed in Equations (11)-(16), the following constraints are applied in the SSRC optimisation model:

$$T_{\mathrm{TES,in}} \leq T_{\mathrm{m,PCM(2,4)}} - 10\ ^{\circ}\mathrm{C} \tag{23}$$

$$T_{\mathrm{TES,out}} \leq T_{\mathrm{m,PCM(1,3)}} \tag{24}$$

$$x_{\mathrm{TES,out}} \geq 1 \tag{25}$$

where $T_{\mathrm{TES,in}}$ is the steam temperature at the TES inlet, $T_{\mathrm{m,PCM(2,4)}}$ the PCM melting temperature of PCM tank 2 or 4, $T_{\mathrm{TES,out}}$ the steam outlet temperature from systems TES-1 and TES-2 during the TES discharging phase, $T_{\mathrm{m,PCM(1,3)}}$ the PCM melting temperature of PCM tank 1 or 3, and $x_{\mathrm{TES,out}}$ the steam quality at the TES outlet.

The constraint in Equation (23) ensures that the temperature differences between the steam and the PCM in the inlets of PCM-2 and PCM-4 tanks are sufficient for effective heat transfer rates. The steam outlet temperatures from PCM-1 and PCM-3 tanks are also limited by the melting temperature of the selected materials as indicated in Equation (24). The PCM temperature could reach to higher temperatures than the melting temperature of the respective material as PCM tanks are charged with steam (heat-source) of higher temperatures (i.e., at least 10 °C higher than the melting temperature of the selected material). However, the average steam outlet temperature from PCM-1 and PCM-3 tanks during the discharging phase is expected, to a large extent, to be less or equal to the melting temperatures of the selected PCMs. The last constraint, Equation (25), is to ensure that the steam condition at the inlet of the turbine is at least saturated vapour to avoid damaging the turbines with very wet steam.

Moreover, the model accounts for TES heat losses to the environment as well as the impact of steam conditions variation (i.e., temperature difference, mass flowrate, pressure, etc.) on the heat transfer rate between the PCM and the steam during charging and discharging modes [60]. Therefore, a charging heat-to-heat efficiency ($\eta_{\mathrm{TES,Ch}}$) of 90% and a discharging heat-to-heat efficiency ($\eta_{\mathrm{TES,Dch}}$) of 90% are assumed (i.e., round-trip efficiency of 81%). Other parameters and steam cycle assumptions are the same as for the PSRC system model, as listed in Table 2. The SSRCs are assumed to operate at full-load conditions most of the time given that the share of each SSRC power output is expected to be only about 2–3% of the total peak power output (i.e., from PSRC and all SSRC systems). Hence, the aggregate SSRC power output can be modulated by switching individual SSRCs on or off when more or less power is required by the electricity grid. Also, the expected decrease in part-load thermal efficiency between SSRCs operating at 100% and at 50% of nominal output is observed to be not greater than 5% (see Section 3.2 for more details). This effect of reduced part-load efficiency is not considered in the paper as it is not expected to have a significant impact on the results. Nevertheless, a more accurate modelling of part-load efficiency variations of the SSRC systems will be addressed in future work.

2.4. Whole-system modelling and inputs

System assessment of flexible nuclear plants is carried out by adopting an extended version of the whole-electricity system investment model (WeSIM), presented in Ref. [30], to include specific features of flexible nuclear generation. Capturing the interactions across various time-scales and asset types at sufficient temporal and spatial granularity is critical when analysing future low-carbon electricity systems. WeSIM is a whole-system analysis model that simultaneously optimises long-term investments into generation, network and storage assets, and short-term operation decisions in order to satisfy the demand at least cost while ensuring adequate security of supply, sufficient volumes of ancillary services and meeting system-wide carbon emission targets [30]. WeSIM can quantify trade-offs between using various sources of flexibility, such as demand-side response (DSR) and energy storage, for real-time balancing and for management of network constraints.

A detailed formulation of the model has been previously provided in Ref. [30]; therefore, only the new and additional elements of the model formulation (i.e., new variables, constraints and parameters) that are relevant for flexible nuclear power plant modelling are presented here. Extensions to the WeSIM model presented here have been implemented in FICO Xpress Optimisation framework [61]. WeSIM is formulated as a large-scale linear programming problem that is solved using the Newton-barrier optimisation algorithm, which identifies the globally optimal solution over the feasible solution space.

2.4.1. Mathematical formulation of the whole-system model

The formulation of the system model presented here assumes a single-node system without considering any distribution, transmission or interconnection assets. A shortened form of the objective function for the mixed-integer linear problem is given in Equation (26). The model minimises the total system cost, which is the sum of annualised investment cost associated with power generation (G), flexible nuclear (N), electrolyser (E), hydrogen storage (H) and battery storage (S) assets, and the annual operating cost across all time intervals considered in the study (in this case all 8760 h of a year). Component investment costs are expressed as products of per-unit cost parameters (π) and decision variables for total capacity (μ). The operating cost term (C) is the function of generation output decision variables (p) and reflects the variable operating costs, no-load costs and start-up costs of thermal generators.

$$\min\{z\} = \sum_{i=1}^{G} \pi_i^G \mu_i^G + \sum_{i=1}^{N} \pi_i^N \mu_i^N + \sum_{i=1}^{E} \pi_i^E \mu_i^E + \sum_{i=1}^{H} \pi_i^H \mu_i^H + \sum_{i=1}^{S} \pi_i^S \mu_i^S + \sum_{t=1}^{\tau} \left(\sum_{i=1}^{G} C_{i,t}^G \left(p_{i,t}^G \right) + \sum_{i=1}^{N} C_{i,t}^N \left(p_{i,t}^N \right) \right) \tag{26}$$

A number of further constraints are formulated in the model (detailed mathematical formulation of the main WeSIM model can be found in Ref. [30] and is omitted here for brevity):

- power supply-balance constraints;
- operating reserve constraints for fast and slow reserves;
- generator operating constraints, including minimum and maximum output, ramping constraints and minimum up and down time constraints;
- annual load factor constraints to account for planned maintenance;
- available energy profiles for variable renewables;
- demand-side response constraints that allow demand shifting;
- emission constraints to limit total annual carbon emissions from the electricity system;
- security of supply constraints.

All variables and constraints presented in the remainder of this subsection represent an extension of the WeSIM model, which in its original formulation does not explicitly consider flexible nuclear plant configurations discussed in this paper.

The number of flexible nuclear units in the system is denoted by n_{FN}, which can be either specified as fixed input or optimised by the model. Unit commitment variables, u, are formulated for each time interval, t, and separately for the PSRC and SSRC components of the flexible nu-

clear units:

$$u_{\mathrm{PSRC},t},\ u_{\mathrm{SSRC},t} \le n_{\mathrm{FN}} \tag{27}$$

In all studies, the PSRC system is assumed to operate as a must-run generator, i.e., that all PSRC units are always in synchronised operation (although not necessarily at full output).

The aggregate heat output of flexible nuclear plant steam generators, $\dot{Q}_{\mathrm{SG},t}$, is bounded from below and above by the product of n_{FN} and the lower and upper bound per one unit:

$$n_{\mathrm{FN}}\ \dot{Q}_{\mathrm{SG}}^{\min} \le \dot{Q}_{\mathrm{SG},t} \le n_{\mathrm{FN}}\ \dot{Q}_{\mathrm{SG}}^{\max} \tag{28}$$

Aggregate power output of PSRC and SSRC components is bounded by the relevant minimum and maximum output levels when these generators are operating:

$$u_{\mathrm{PSRC},t}\ \dot{W}_{\mathrm{PSRC}}^{\min} \le \dot{W}_{\mathrm{PSRC},t} \le u_{\mathrm{PSRC},t}\ \dot{W}_{\mathrm{PSRC}}^{\max} \tag{29}$$

$$u_{\mathrm{SSRC},t}\ \dot{W}_{\mathrm{SSRC}}^{\min} \le \dot{W}_{\mathrm{SSRC},t} \le u_{\mathrm{SSRC},t}\ \dot{W}_{\mathrm{SSRC}}^{\max} \tag{30}$$

Note that the multiple modules of TES-SSRC units discussed in the previous section are treated aggregately in this formulation. The rates of charging and discharging heat into/from the TES systems are given by:

$$\dot{Q}_{\mathrm{TES,Ch},t} \le n_{\mathrm{FN}}\ \dot{Q}_{\mathrm{TES,Ch}}^{\max} \tag{31}$$

$$\dot{Q}_{\mathrm{TES,Dch},t} \le n_{\mathrm{FN}}\ \dot{Q}_{\mathrm{TES,Dch}}^{\max} \tag{32}$$

The energy content of TES is limited by the aggregate storage size, while the TES balance equation accounts for charging and discharging heat subject to losses:

$$Q_{\mathrm{TES},t} \le n_{\mathrm{FN}}\ Q_{\mathrm{TES}}^{\max} \tag{33}$$

$$Q_{\mathrm{TES},t} = Q_{\mathrm{TES},t-1} + \left(\eta_{\mathrm{TES,Ch}}\ \dot{Q}_{\mathrm{TES,Ch},t} - \frac{1}{\eta_{\mathrm{TES,Dch}}}\ \dot{Q}_{\mathrm{TES,Dch},t}\right)\ \delta \tag{34}$$

Heat balance constraints are formulated to ensure that the heat produced by steam generator is used either directly in the PSRC unit or partially stored in TES, while any heat released from TES is used to power the SSRC units:

$$\dot{Q}_{\mathrm{SG},t} - \dot{Q}_{\mathrm{TES,Ch},t} = \dot{Q}_{\mathrm{PSRC},t} = \beta_{\mathrm{PSRC}}\ u_{\mathrm{PSRC},t} + \gamma_{\mathrm{PSRC}}\ \dot{W}_{\mathrm{PSRC},t} \tag{35}$$

$$\dot{Q}_{\mathrm{TES,Dch},t} = \dot{Q}_{\mathrm{SSRC},t} = \beta_{\mathrm{SSRC}}\ u_{\mathrm{SSRC},t} + \gamma_{\mathrm{SSRC}}\ \dot{W}_{\mathrm{SSRC},t} \tag{36}$$

The link between the input heat and output electricity for PSRC and SSRC units in Equations (35) and (36) is formulated by assuming a no-load heat rate, β, that is incurred whenever the unit is operating regardless of the output level, and incremental heat rate, γ, that multiplies the generator output level. These heat rate parameters are estimated from the results of thermodynamic modelling presented earlier in this section. Other operating constraints such as ramping and minimum up/down times were also implemented in the model but are omitted here for brevity.

Finally, the annual availability constraint for the steam generator output is formulated based on the product of the annual availability factor, α_{FN}, and the duration of the year in hours, τ,:

$$\sum_{t=1}^{\tau} \dot{Q}_{\mathrm{SG},t} \le n_{\mathrm{FN}}\ \dot{Q}_{\mathrm{SG}}^{\max}\ \tau\ \alpha_{\mathrm{FN}} \tag{37}$$

The total operation cost of flexible nuclear units contributing to total system cost in Equation (26) is simply equal to the product of total SG output and the cost of nuclear fuel.

2.4.2. Assessing the value of flexible nuclear units in low-carbon electricity systems

System value of flexible nuclear generation in this paper has been quantified as a *whole system benefit* from replacing a standard nuclear unit with a flexible alternative that also includes TES and SSRC generation. In the first step, the whole-system model is run to minimise the total system cost and construct a series of *counterfactual* scenarios in which nuclear generation had no added flexibility features. In the second step, a series of model runs was performed with nuclear units being replaced with flexible nuclear configurations that included TES and SSRC generation. Any resulting reduction in total system cost (but not reflecting the cost of making the nuclear generation more flexible) is then interpreted as whole system benefit of flexible nuclear.

Whole system benefit of flexible nuclear is a useful benchmark to compare against the estimated cost of this increased flexibility through TES and a secondary steam cycle. This comparison is provided in the results section, with the aim of identifying those electricity system features that result in a positive net benefit of flexible nuclear generation.

2.4.3. Scenarios used for assessing the value of flexible nuclear generation

In order to examine the key drivers for the system value of flexible nuclear, a number of scenarios have been run for different inputs assumptions. Two generic systems have been assumed, North and South, both sized to approximately match the UK electricity system. Although the annual demand volume in both systems was the same, around 400 TWh_{el}, the North system had a higher share of electrified heating demand then South, but a lower share of cooling demand. Also, in the North system it was assumed that onshore and offshore wind were available at relatively higher capacity factors (40% and 54%, respectively), while for solar PV the capacity factor was only 14%. In contrast, in the South the assumed solar PV capacity factor was 24%, while wind capacity factors were lower than in the North (35% and 49% for onshore and offshore, respectively). In all case studies except one it was assumed that there is exactly one nuclear unit in the system, with the PSRC rating of 1610 MW_{el}. This unit was assumed to be either conventional (in the counterfactual studies) or equipped with TES and SSRC units in the flexible studies.

For each of the two systems (North and South) a series of scenarios was investigated, as listed in Table 4, by running both counterfactual and flexible nuclear studies. The purpose of these scenarios was to explore the impact of various assumptions on the system benefit of flexible nuclear, including the level of system carbon emissions, number of nuclear units in the system, variations in SSRC duration (ratio between TES size and maximum SSRC heat intake; default assumption was 1 h), uptake and cost of battery energy storage system (BESS) and demand side response (DSR), and the ability to invest in carbon offsets such as bioenergy with carbon capture and storage (BECCS).

3. Results and discussion

The thermodynamic performance of the PSRC system during full and part-load operations is discussed in Sections 3.1 and 3.2. The results of the designed TES-SSRC modular units are presented and discussed in Section 3.3. Sections 3.4 to 3.6 highlight the benefits of added flexibility, the impact of flexible nuclear on cost-optimised technology capacity

Table 4
List of system scenarios used for quantifying system benefits of flexible nuclear.

ID	Scenario description
A	Net zero carbon system
B	Carbon intensity target of 25 gCO_2/kWh
C	Carbon intensity target of 50 gCO_2/kWh
D	5 nuclear units instead of one
E1	SSRC duration of 0.5 h
E2	SSRC duration of 2 h
E3	SSRC duration of 4 h
F	Higher cost of BESS (50% higher than baseline)
G	Low DSR uptake of 25% (vs. 50% used in other cases)
H	No investment in carbon offsets (BECCS)

Table 5
Obtained PSRC system steam parameters at nominal power.

Parameter	Value
HPT main outlet pressure (kPa)	2390
HPT main outlet temperature (°C)	221
Reheater main inlet mass flowrate (kg/s)	1880
Reheater outlet temperature (°C)	289
LPT main outlet pressure (kPa)	10
LPT main outlet mass flowrate (kg/s)	1370
Condensate pump outlet pressure (kPa)	2390
Net electrical power (MW_{el})	1610
Cycle efficiency (%)	35.7

mix, and the operation of flexible nuclear power plants in low-carbon electricity systems.

3.1. Performance of the primary steam Rankine cycle system at nominal load

The main operating parameters of the PSRC system that result in maximum cycle efficiency at nominal power are listed in Table 5. The temperature-specific entropy (*T-s*) diagram illustrating the main thermodynamic processes of the PSRC is shown in Fig. 2.

The calculated steam generator outlet temperature is 294 °C at 7800 kPa, which represents a slightly superheated steam. The steam enters the HPT at the same conditions and expands to 2390 kPa, reheated to 289 °C in the reheater, and then continue expanding in the LPT to a condensing pressure of 10 kPa. The calculated net electrical power is 1610 MW_{el}, which is 1.2% less than the declared design net capacity of 1630 MW_{el} of EPR [34]. Such difference is expected since the actual EPR steam cycle parameters and components might be different to what is assumed in this study. The obtained maximum heat-to-electricity efficiency of the PSRC system is 36%, which is equivalent to a heat rate of 10.1 GJ/MWh_{el}. This efficiency is relatively high compared to other PWRs designs (an average of 33%) but it is achievable with recent improvements in component efficiencies [62].

3.2. Performance of the primary steam Rankine cycle system during part-load operation mode (charging mode)

The nominal operating conditions (i.e., design isentropic efficiencies, mass flowrate, pressure, and temperature of both turbines) of the PSRC

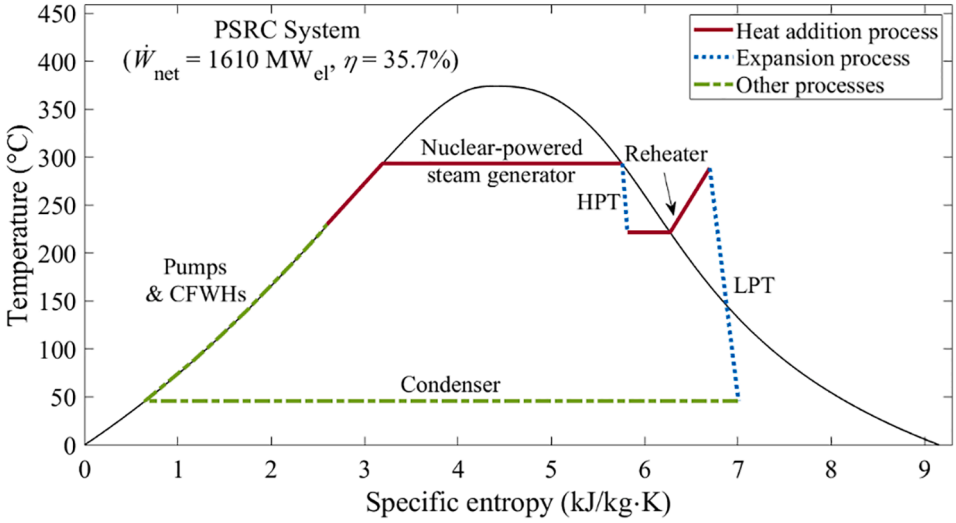

Fig. 2. Temperature-specific entropy, *T-s*, diagram showing the thermodynamic processes of the efficiency optimised PSRC system during nominal load operation.

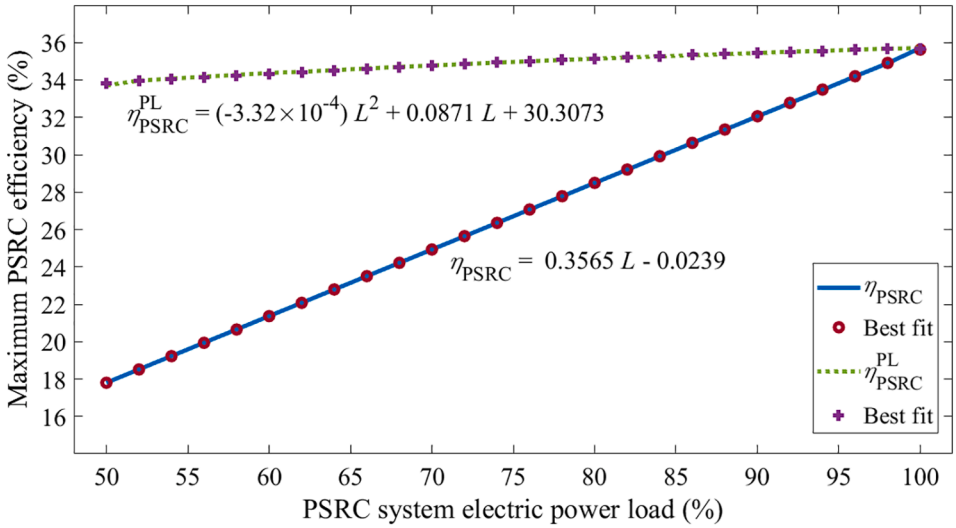

Fig. 3. Maximum PSRC system efficiency for electric loads from 50% to 100% of nominal power. Parameter (*L*) in the obtained best fit correlations is the PSRC system power load in %.

system are extracted to run the part-load PSRC system model using Equations (17) and (18). Fig. 3 presents the maximum obtained cycle efficiencies, as defined in Equations (9) and (19), from 50% to 100% of nominal power (i.e., from 806 to 1610 MW_{el}). The PSRC system efficiency ranges from 18% at 50% power load to 36% at 100% power load. The trend is linear since the rate of heat addition is constant for all power loads (i.e., reactor is operating at maximum thermal power level). However, the part-load PSRC system efficiency is higher for all loads, ranging from 34% at 50% power load to 36% at maximum load. The difference is less than 2% and mainly due to the decrease of turbine isentropic efficiency at part-load operations. Moreover, best fit lines are constructed for both PSRC system efficiency indicators in order to allow estimating the PSRC system efficiency and the incremental heat rate required by the whole-system model.

3.3. Performance of thermal energy storage and secondary steam Rankine cycle systems (discharging mode)

The calculated average amount of stored heat in each TES-SSRC module is 390 MWh_{th} (i.e., in all TES-1 and TES-2 tanks). This is calculated from charging thermal power of 217 MW_{th} lasting 1 h and the assumed 90% heat-to-heat charging efficiency for TES-1 and for TES-2. In this study, it is assumed that 5 TES-SSRC modules are installed. Therefore, the calculated total amount of stored heat in the 5 modules is 1950 MWh_{th}.

Results obtained from the efficiency optimisation model of systems SSRC-1 and SSRC-2 are summarised in Table 6. The temperature-specific entropy (*T-s*) diagrams illustrating the thermodynamic processes of systems SSRC-1 and SSRC-2 are presented in Fig. 4a and Fig. 4b, respectively. The steam inlet temperature is 132 °C for both cycles. However, the boiling (i.e., saturation) steam pressure at the TES inlet is higher for system SSRC-1 since steam is boiled at a temperature of 272 °C, which is 10 °C below the melting temperature of PCM-1. For system SSRC-2, the maximum temperature is 208 °C and steam is boiled at 198 °C (saturation pressure of 1490 kPa). System SSRC-1 delivers 57.6 MW_{el} of net electric power, resulting in a cycle efficiency of 30%, while system SSRC-2 generates 46.3 MW_{el} of electric power at 24% of cycle efficiency. Although system SSRC-2 efficiency is relatively high, it operates at low pressure and temperature ranges that are not recommended for steam Rankine cycles. Thus, other working fluids such as organic fluid will be considered and compared with steam in future research. The total amount of electrical power from one TES-SSRC module is 104 MW_{el}, which results in 520 MW_{el} output if all 5 installed modules are simultaneously discharging at full rated power capacity. Hence, the maximum power output of the proposed configuration is 2130 MW_{el} (1610 MW_{el} from the PSRC and 520 MW_{el} from the SSRCs), which is 32% higher than the nominal PSRC system power output. The electricity-to-electricity roundtrip efficiency, which is defined as the amount of electricity generated from all SSRC systems (520 MWh_{el}) divided by the amount of electricity that could be generated from the PSRC system (805 MWh_{el}) during the TES charging phase is 64%.

Table 6
Main operating parameters of SSRC systems for 1 h discharging duration.

Parameter	SSRC-1	SSRC-2
TES discharging thermal power (MW_{th})	195	195
TES steam inlet temperature (°C)	132	132
TES steam outlet temperature (°C)	282	208
TES steam mass flowrate (kg/s)	77.2	77.5
TES steam inlet pressure (kPa)	5680	1490
Condensing pressure (kPa)	10	10
Reheater outlet temperature (°C)	277	203
Net electrical power (MW_{el})	57.6	46.3
Cycle efficiency (%)	29.6	23.7

3.4. Benefits of flexible nuclear in low-carbon electricity systems

The results of whole system benefit assessment of flexible nuclear across the two systems considered in this study are shown in Fig. 5 and Fig. 6, for the North and South systems, respectively. The two systems are characterised by different shares of wind and solar PV generation and different seasonal demand variations. The system benefits represent annualised system cost savings across different scenarios, based on annualised values for asset investment costs and annual operating costs. For all cases, system benefits are broken down into various cost components, including generation investment, operating cost (OPEX), storage investment, electrolyser investment and hydrogen storage investment. Note that the system benefits are always expressed per one flexible nuclear unit (with a PSRC system size of 1610 MW_{el}), so that in Scenario D with 5 flexible nuclear units the total system benefit was divided by 5 (other scenarios only assumed a single flexible nuclear unit). These benefits can be compared to the costs required to achieve the enhanced flexibility, i.e., the additional investment cost of TES-SSRC modules.

The key conclusions from the system benefit results are as follows:

- System benefit of flexible nuclear generally consists of multiple components, indicating that the enhanced flexibility of nuclear plants can displace alternative flexibility options such as battery and hydrogen storage with electrolysers, as well as the investment and operating cost of generation capacity. The compound benefit of nuclear flexibility can sometimes have negative components (e.g., the generation component) due to the reconfiguration of the rest of the generation mix and changes in its output, but those are more than offset by positive cost savings in other components.
- The benefit increases with more stringent carbon emission targets, from £60.1–63.1m/yr with 50 gCO_2/kWh to £67.4–74.3m/yr for a net-zero carbon system.
- System values observed in the North system tend to be slightly higher than in the South system if the TES-SSRC duration is 1 h. This can be explained by the higher PV and lower wind penetration in the South, and the need for longer-term flexibility (i.e., over multiple hours) to compensate for the variability of PV generation when compared to wind. For the same reason, a higher system value is observed in the South system with 4-h duration of the TES-SSRC unit.
- System benefits diminish with a larger number of nuclear units, so that with 5 flexible units the benefit per one unit is only about a third of the benefit achieved by a single unit (but still providing higher aggregate benefit for all 5 units of flexible nuclear).
- Increasing the power-to-energy ratio of SSRC generators for the same TES size results in significantly higher system benefits, and *vice versa*, but on the other hand also increases the cost of the flexible nuclear assets.
- Increasing the cost of battery storage (BESS) results in a marginally higher benefit of flexible nuclear (£75.1m/yr in the North and £69.9m/yr in the South), while reducing the uptake of DSR does not appear to have a material impact on the system value of flexible nuclear.
- Preventing the model to invest into BECCS carbon offsets tends to reduce the system value of flexible nuclear, which now has to compete with biomass and hydrogen generation in the counterfactual case, rather than with CCS and CCGT generation combined with carbon offsets.

Fig. 7 and Fig. 8 show the comparison of system net benefits with an estimate of the investment cost of enhanced flexibility for the North and the South systems, respectively. Maroon squared dots in Fig. 7 and Fig. 8 represent the estimated cost values (i.e., investment costs of flexible nuclear) for each scenario, while black dots are for the total system benefit. The net system benefits are presented by the blue bars, which is the difference between the total system benefit and the estimated cost of

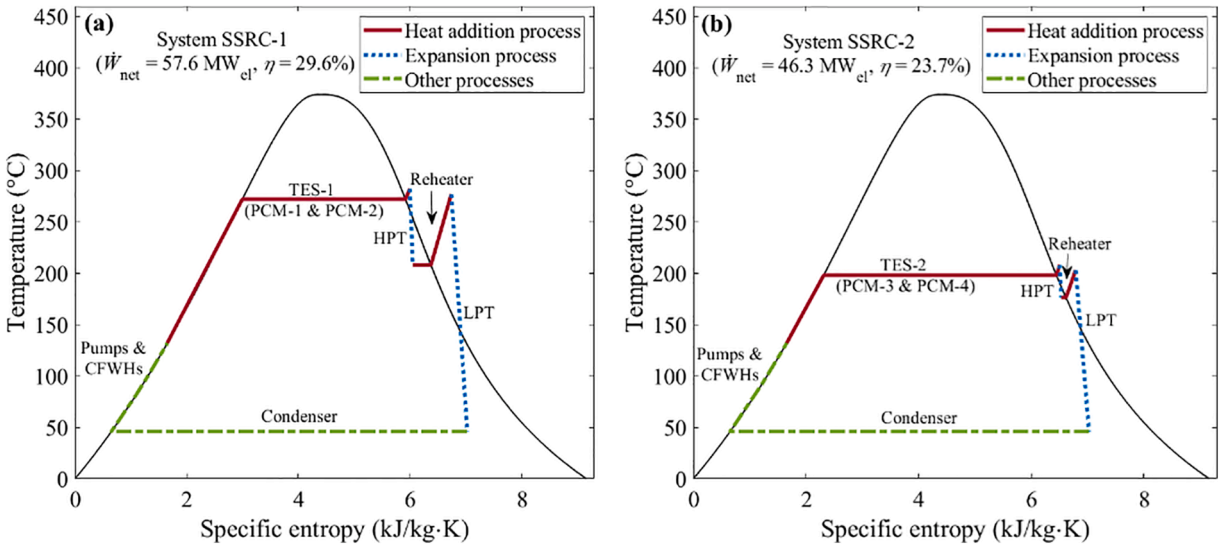

Fig. 4. Temperature-specific entropy, *T-s*, diagrams indicating the thermodynamic processes of the efficiency optimised SSRC systems. (a) is for system SSRC-1 and (b) is for system SSRC-2.

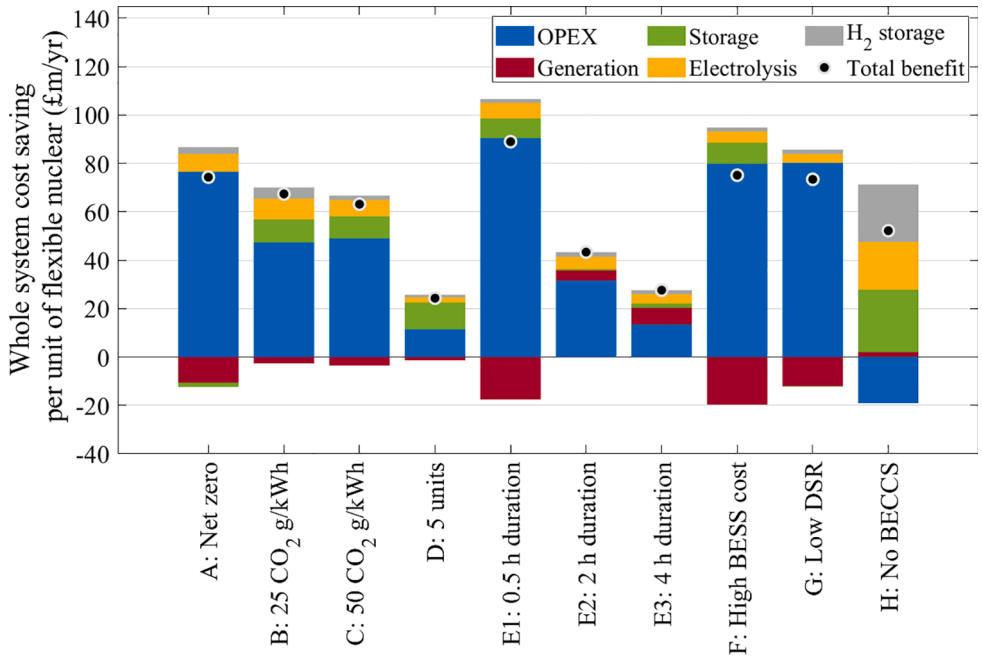

Fig. 5. Whole system benefit of flexible nuclear across scenarios in the North system. Different components in stacked column charts represent changes in different system cost categories. Black dots represent total system benefits. The scenarios are described in Table 4 of Section 2.4.3.

flexibility.

The estimated cost values are calculated based on the average cost of TES of £25/kWh_{th} [63], and the cost of SSRC systems of £965/kW_{el} [64]. With these assumptions the annualised cost of added flexibility is estimated at £42.7m/yr per one unit with the default duration assumption for the TES-SSRC component of 1 h. This cost increases to £81.5m/yr for 0.5-h duration and drops to £23.3m/yr and £13.5m/yr for 2-h and 4-h durations, respectively. At these cost estimates the flexibility upgrade appears to be cost-efficient (i.e., its benefits exceeding the cost) in all cases for both systems (i.e., North and South) except with 5 units added to the system instead of one. The highest net benefit (i.e., the difference between total benefit and cost) is observed in the net zero and high BESS cases, at £31.6–32.4m/yr in the North system and £24.7–27.3m/yr in the South system.

3.5. Impact of flexible nuclear on cost-optimal technology capacity mix

The breakdown of installed power generation capacity by technology obtained from the whole-system model for the North and South systems are shown in Fig. 9 and Fig. 10, respectively. In both figures, (a) represents the installed capacities for the baseline case (i.e., without flexible nuclear), while (b) corresponds to the changes of those capacities after replacing the conventional nuclear plant with a flexible one across all scenarios. Each colour in the stacked columns represents a different power generation technology as shown in the right-hand side legends of Fig. 9 and Fig. 10.

The capacity mix of the North system (Fig. 9a) is dominated by onshore and offshore wind due to their favourable economics, along with a sizeable volume of solar PV capacity. In the South system

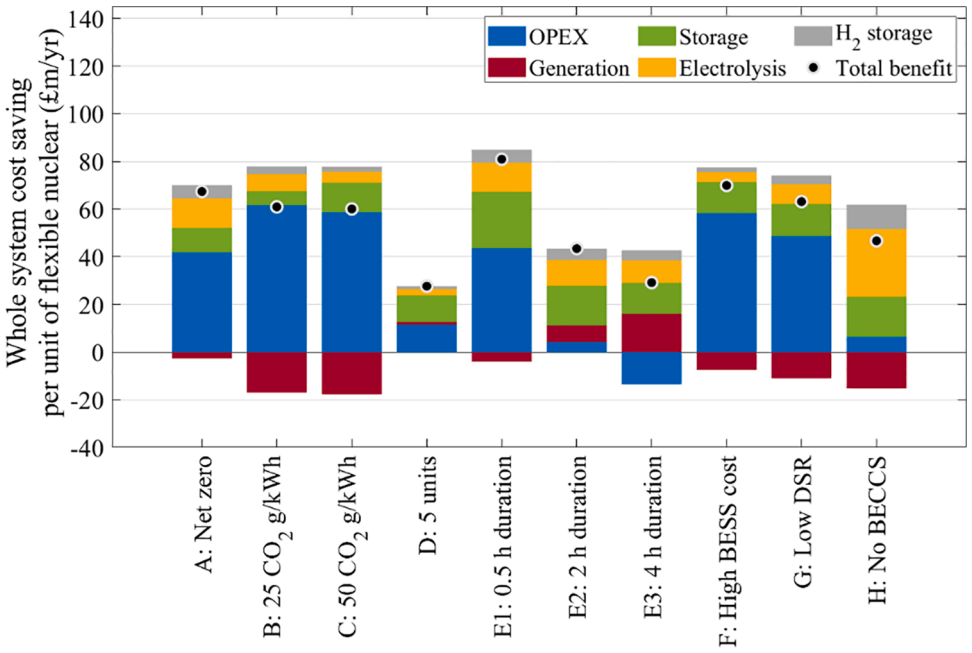

Fig. 6. Whole system benefit of flexible nuclear across scenarios in the South system. Different components in stacked column charts represent changes in different system cost categories. Black dots represent total system benefits. The scenarios are described in Table 4 of Section 2.4.3.

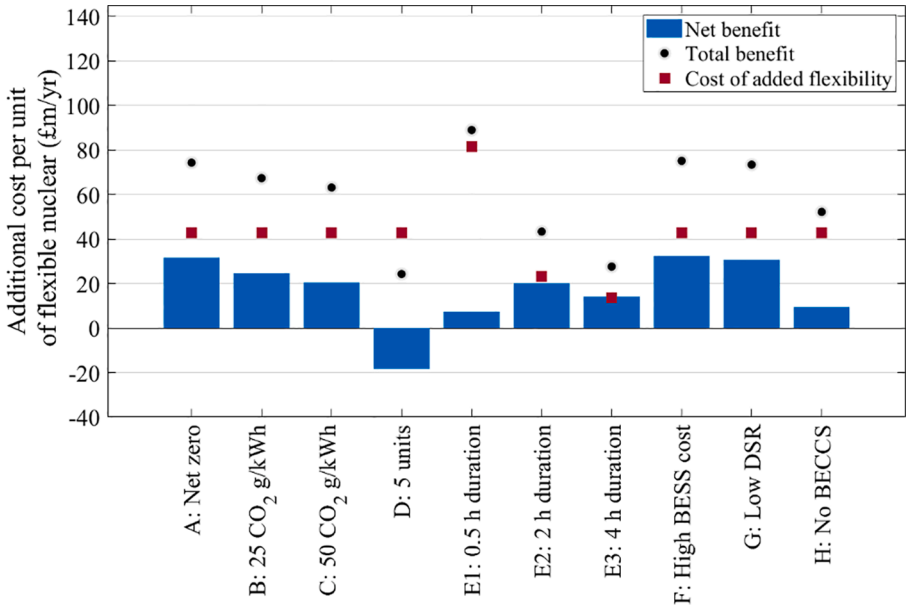

Fig. 7. Net system benefit of flexible nuclear across scenarios in the North system calculated using total system benefits and cost of added flexibility of nuclear plants (i.e., investment cost of flexible nuclear). The scenarios are described in Table 4 of Section 2.4.3.

(Fig. 10a) the main source of power is solar PV generation because of a higher capacity factor than in the North system. To help with cost-effective integration of variable renewable generation, in both North and South there is a significant volume of battery storage (between 75 and 112 GW_{el} in Scenario A in North and South, respectively). Also, in both systems, with the exception of Scenario H, the generation portfolio includes about 30–35 GW_{el} of gas CCGT generation capacity that is split between conventional CCGT and CCS plant in roughly similar proportions for net zero scenarios (A, D, F and G). In Scenarios B and C, the share of unabated CCGT generation increases due to a less restrictive carbon emission constraint. To meet the net zero carbon target, Scenarios A, D, F and G also include a relatively small amount (0.6–1 GW_{el}) of BECCS capacity that acts as carbon offset and compensates for any emissions from CCGT and gas CCS plants. In Scenario H, where BECCS is not allowed to be built, the model no longer adds any CCGT or gas CCS capacity (as it is not able to offset their carbon emissions), but rather increases the amount of wind, solar PV and battery storage capacity, also accompanied by extra biomass and hydrogen CCGT capacity to provide firm zero-carbon generation.

Fig. 9b and Fig. 10b show how the cost-optimal capacity mix changes when the nuclear units in the system are made more flexible by adding TES and SSRC components. The most obvious change is the increase in generation capacity of nuclear plant, which follows directly from adding the SSRC generation cycle. Although there are many complex interactions in the impact of flexible nuclear on the technology mix, there is a general trend that making nuclear more flexible increases the

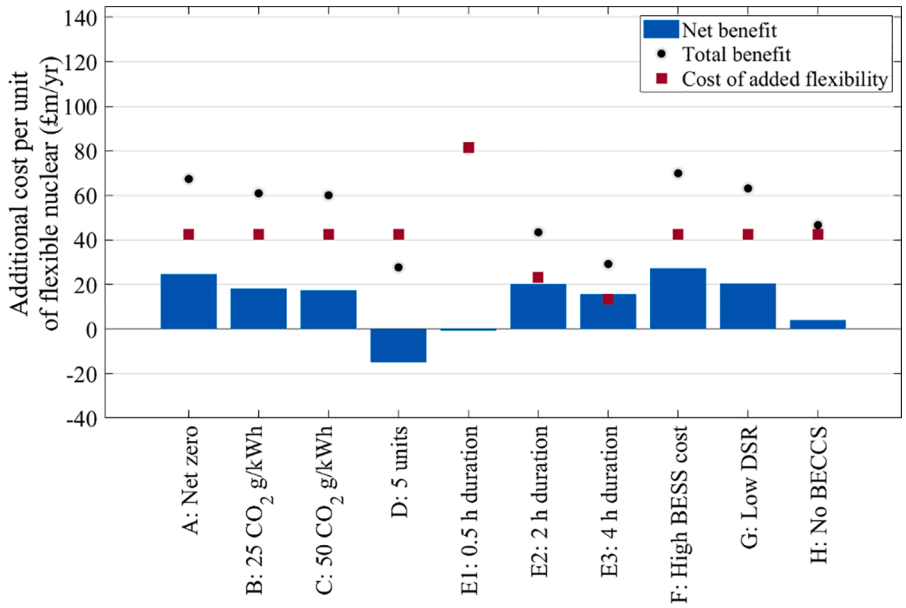

Fig. 8. Net system benefit of flexible nuclear across scenarios in the South system calculated using total system benefits and cost of added flexibility of nuclear plants (i.e., investment cost of flexible nuclear). The scenarios are described in Table 4 of Section 2.4.3.

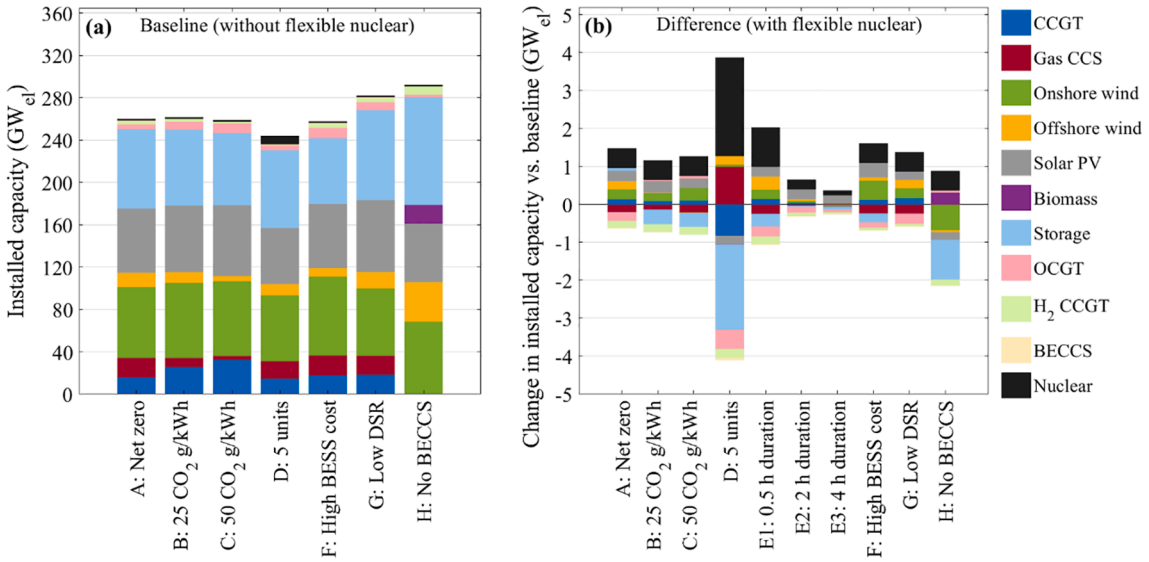

Fig. 9. (a) Installed power capacity of conventional nuclear power with the other power generation technologies (i.e., baseline), and (b) changes in installed capacity with flexible nuclear in the North system for the considered scenarios that are described in Table 4 of Section 2.4.3. The results for Scenarios E1, E2 and E3 are obtained relative to Scenario A.

capacity of wind and solar PV and to a smaller extent gas CCGT, while reducing the capacity of gas CCS, hydrogen CCGT and battery storage. This is driven by the increased flexibility of nuclear, which both increases the capability of the system to cost-effectively integrate variable renewables, and on the other hand reduces the requirements for other means of flexibility such as battery storage, or dispatchable low-carbon generation such as gas CCS or hydrogen CCGT. Note that the utilisation of flexible nuclear will inevitably lead to some energy losses due to storing and releasing heat from the TES system, which means that at an annual level more electricity needs to be generated, and the least-cost solution suggests this should be mostly done using renewables.

In Scenario H, where BECCS is not allowed as an option, flexible nuclear reduces the need for producing hydrogen from electrolysis and using it in hydrogen CCGT generation. Some of the hydrogen generation is replaced by a slight increase in the capacity of biomass generation. Lower electricity requirements for electrolysis also lead to a net reduction in renewable generation capacity in that scenario as well as lower requirements for battery storage.

3.6. *Operation of flexible nuclear power plant*

The utilisation of individual components of a flexible nuclear plant on an hourly basis are illustrated in Fig. 11 and Fig. 12. The example shown in Fig. 11 represents a winter week in the North system, while the one shown in Fig. 12 represents a summer week in the South system. Both figures include hourly profiles for SG heat output, power output from PSRC and SSRC systems, and net heat output from TES (difference between discharging and charging). To help identify key drivers for the operating patterns of flexible nuclear, the chart also presents the level of net demand in the system, which is obtained as the difference between

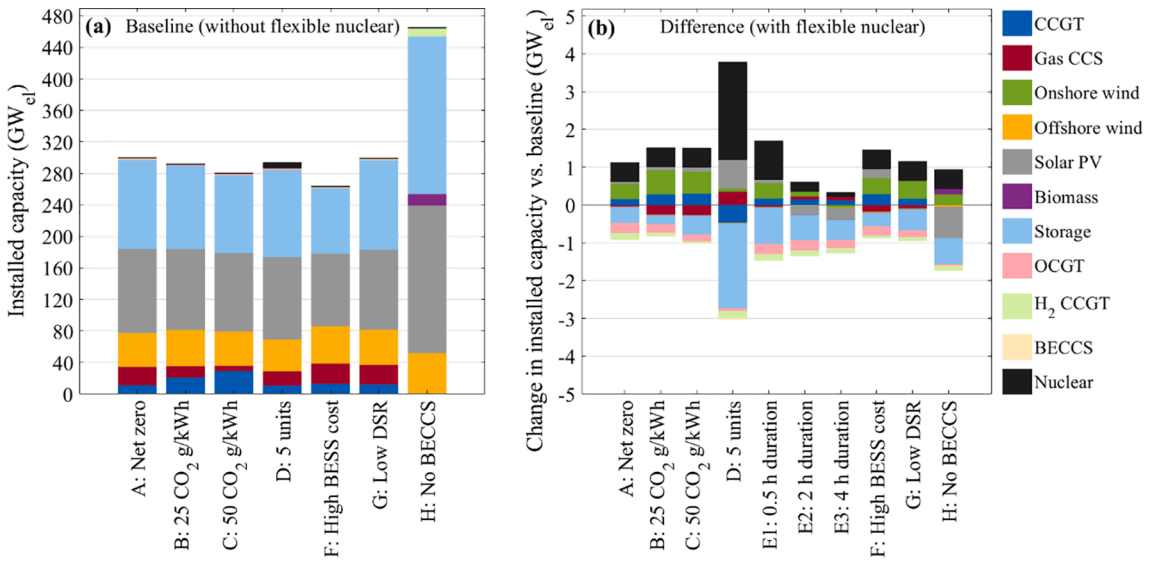

Fig. 10. (a) Installed power capacity of conventional nuclear power with the other power generation technologies (i.e., baseline), and (b) changes in installed capacity with flexible nuclear in the South system for the considered scenarios that are described in Table 4 of Section 2.4.3. The results for Scenarios E1, E2 and E3 are obtained relative to Scenario A.

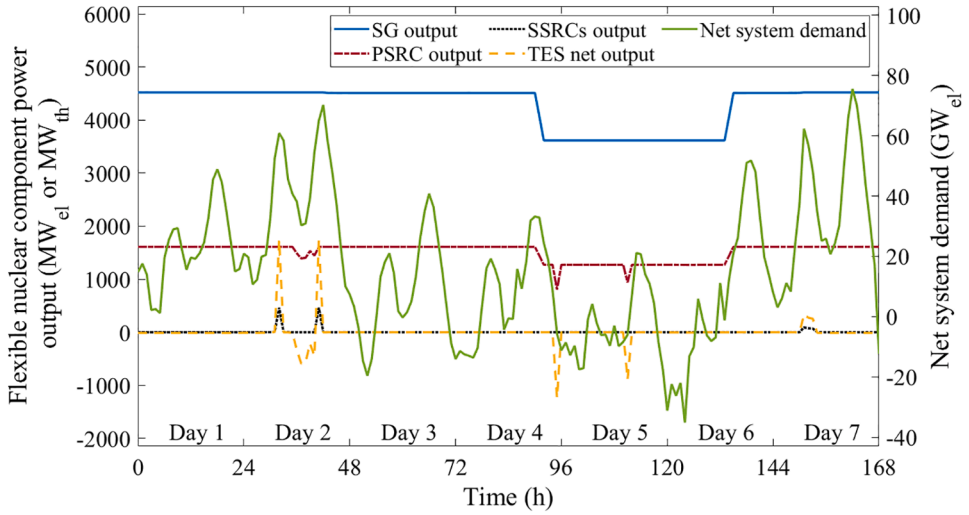

Fig. 11. Hourly operation of flexible nuclear generation during a winter week in the North system. Net system demand represents the difference between system demand and total wind and solar PV output, and is plotted against the right-hand axis.

total system demand (before any DSR or battery storage actions) and total variable renewable output, which included onshore and offshore wind and solar PV generation.

As expected, the SSRC generation is activated only during periods of high net demand (i.e., during periods of low renewable output) when energy in the system is scarce, which in the example shown in Fig. 11 occurs on the second and seventh day of the week. Note that SSRC generator is not always operating during high net demand conditions given that there are other forms of flexibility (DSR and battery storage) with time-varying availability that are also optimised by the model. Heat stored in TES units is replenished during periods of relatively lower net demand, which is observed at midday on Day 2, and around midnight and midday on Day 5. Also note that during Days 5 and 6 the supply of renewable electricity is so abundant that it results in very low or even negative net demand. The SG output on those days is therefore adjusted downwards by 20% (corresponding to the lowest allowed operating point), and so is the PSRC system output, which is further reduced down to 50% of nominal output during those hours when heat is stored into TES units.

In the South system during the summer (i.e., example shown in Fig. 12), the net demand follows a regular pattern of being high during the night and low or even negative during the day, due to high solar PV output in the South. Similar to the North system, the SSRC generators are activated during high demand periods, while TES charging takes place when the net demand is low and there is excess electricity produced by solar PV generation. It is also observed that the thermal power output from the PSRC system is reduced by 20% during low demand periods around midday and further reduced to 50% of nominal power when charging the TES units.

4. Conclusions

A combined thermoeconomic (i.e., thermodynamic and economic) analysis of an upgraded nuclear power plant coupled with thermal energy storage (TES) and secondary power generators was presented. The analysis also included a quantification of the benefits of operating such

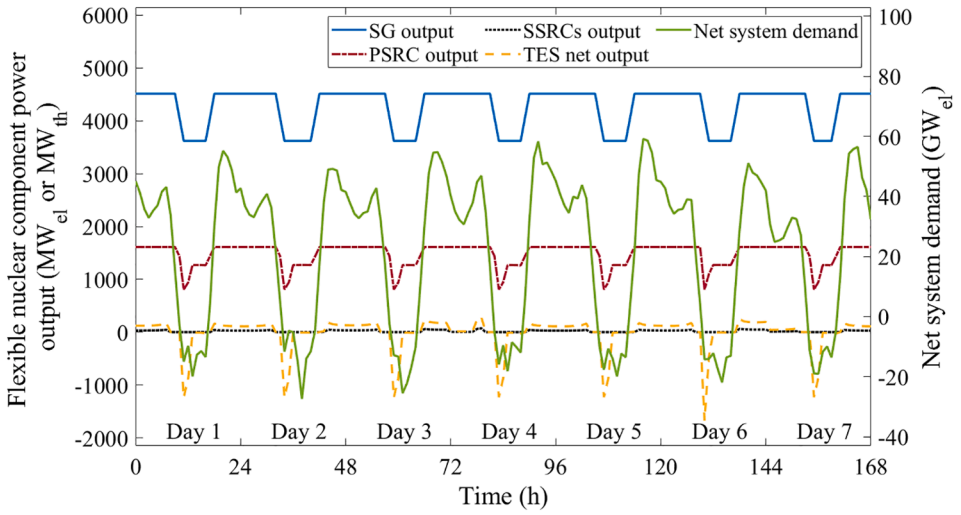

Fig. 12. Hourly operation of flexible nuclear generation during a summer week in the South system. Net system demand represents the difference between system demand and total wind and solar PV output, and is plotted against the right-hand axis.

flexible nuclear power plants in a low-carbon electricity UK system, with results transferable to electricity infrastructure similar to that of the UK. The thermodynamic modelling and optimisation framework presented here allow for the identification of the optimal operating conditions of the primary power generation system during both nominal load and part-load operations, as well as for the determination of the technical design constraints of the proposed modular TES and secondary steam Rankine cycle (SSRC) units. Moreover, the whole-system electricity model enables a quantification of the system value of the enhanced flexibility that such nuclear plants can offer in the context of decarbonising the electricity supply with a high share of variable renewables.

The thermodynamic performance of the primary steam Rankine cycle (PSRC) system of the considered nuclear power plant (EPR) was investigated during nominal load and part-load operation by taking in consideration the operation of steam turbines at off-design conditions. Results revealed a maximum PSRC thermal efficiency of 36% at 100% power output, which decreased to 34% at 50% power output while the TES charging process was performed, mainly due to the reduced turbine isentropic efficiencies at off-design condition. Moreover, performance predictions showed that the proposed configuration of adding flexibility through the coupling with PCM-based TES and SSRC systems has the potential to increase overall power output during peak load by 32% (relative to the baseload nuclear plant's nominal rated power) during full TES discharge mode, from 1610 MW_{el} to 2130 MW_{el}, with an overall electricity-to-electricity roundtrip efficiency of 64%, and 520 MW_{el} of additional peak power being generated by the 5 installed TES-SSRC modular units. The peak power output can be further increased where additional TES-SSRC modules are installed (i.e., more than 5) or when the SSRC generators are sized with a higher power-to-energy ratio utilising the current TES system capacity.

The whole-system economic benefits of a such flexible nuclear plants was quantified by the reduction in the total system electrical infrastructure cost resulting from replacing conventional with flexible nuclear plants for several scenarios in the context of the UK's national electricity system. Two generic systems were analysed: North and South (i.e., with different wind and solar PV capacity factors and seasonal demand variations), both sized to approximately match the UK's electricity system with an annual generated electricity of 400 TWh_{el}. Economic benefits of up to about £75m/yr were identified in the majority of the analysed scenarios, which equates to almost £1 b in capitalised benefits of flexibility over the lifetime of a single plant. Moreover, the highest net benefit (i.e., the difference between total benefit and the cost of added flexibility of £42.7m/yr for 1-h TES discharge duration) was observed in the net zero and high BESS scenarios, at £31.6–32.4m/yr in the North system and £24.7–27.3m/yr in the South system. Nevertheless, the value was found to vary considerably with system characteristics such as the composition of the low-carbon generation mix, carbon target, level of flexibility, and plant parameters such as SSRC duration. This suggests that the value of this technology will be system-dependent, and that system characteristics should be adequately considered when evaluating the benefits of different flexible nuclear plant configurations and choosing the most cost-effective designs and operational characteristics.

Future work related to the proposed flexible nuclear power plant configuration will include: (i) investigation of other technically feasible steam extraction points from the PSRC system for charging the TES system; (ii) assessment of different working fluids for the secondary power generation cycles; (iii) detailed modelling and sizing of the PCM tanks including thermodynamic analysis of TES system charge/discharge dynamics; (iv) investigation of the feasibility for multiple uses of the stored heat to match heating demand and operate thermally driven processes for hydrogen storage, water splitting or synthetic fuels production; and (v) cost-optimisation of the size of individual components from the system perspective.

CRediT authorship contribution statement

Abdullah A. Al Kindi: Conceptualization, Data curation, Formal analysis, Methodology, Software, Validation, Visualization, Writing – original draft, Writing – review & editing. **Marko Aunedi:** Data curation, Formal analysis, Methodology, Software, Validation, Writing – original draft, Writing – review & editing. **Antonio M. Pantaleo:** Conceptualization, Formal analysis, Methodology, Writing – review & editing. **Goran Strbac:** Conceptualization, Funding acquisition, Project administration, Resources, Supervision. **Christos N. Markides:** Conceptualization, Funding acquisition, Methodology, Project administration, Resources, Supervision, Writing – review & editing.

Declaration of Competing Interest

The authors declare that they have no known competing financial interests or personal relationships that could have appeared to influence the work reported in this paper.

Acknowledgements

This work was supported by the UK Engineering and Physical Sciences Research Council (EPSRC) [grant numbers EP/P004709/1, EP/R045518/1, and EP/S032622/1] and by the Government of the Sultanate of Oman. Data supporting this publication can be obtained on request from cep-lab@imperial.ac.uk. For the purpose of Open Access, the authors have applied a CC BY public copyright licence to any Author Accepted Manuscript version arising from this submission.

References

[1] International Atomic Energy Agency (IAEA). Climate Change and Nuclear Power. 2020.
[2] Department of Business. Energy & Industrial Strategy. Nuclear Industrial Strategy – The UK 's Nuclear Future. 2013.
[3] Department of Business, Energy & Industrial Strategy. Climate Change Act 2008 (2050 Target Amendment) Order 2019, https://www.legislation.gov.uk/uksi/2019/1056/made [accessed 13 April 2021].
[4] Jenkins JD, Zhou Z, Ponciroli R, Vilim RB, et al. The benefits of nuclear flexibility in power system operations with renewable energy. Appl Energy 2018;222:872884.
[5] Denholm P, King JC, Kutcher CF, Wilson PPH. Decarbonizing the electric sector: Combining renewable and nuclear energy using thermal storage. Energy Policy 2012;44:301–11.
[6] Carlson F, Davidson JH, Tran N, Stein A. Model of the impact of use of thermal energy storage on operation of a nuclear power plant Rankine cycle. Energy Convers Manag 2019;181:36–47.
[7] Park JH, Heo JY, Lee JI. Techno-economic study of nuclear integrated liquid air energy storage system. Energy Convers Manag 2022;251:114937.
[8] Amuda KF, Field RM. Nuclear heat storage and recovery for the APR1400. J Energy Storage 2020;28:101171.
[9] Kluba A, Field R. Optimization and exergy analysis of nuclear heat storage and recovery. Energies 2019;12:4205.
[10] Alameri SA. A coupled nuclear reactor thermal energy storage system for enhanced load following operation. Ph.D. Dissertation. Colorado School of Mines, Colorado, USA. 2015.
[11] Forsberg CW, Stack DC, Curtis D, Haratyk G, Sepulveda NA. Converting excess low-price electricity into high-temperature stored heat for industry and high-value electricity production. Electr J 2017;30:42–52.
[12] Forsberg C. Hybrid systems to address seasonal mismatches between electricity production and demand in nuclear renewable electrical grids. Energy Policy 2013;62:333–41.
[13] Forsberg CW. Heat in a bottle. ASME Mechanical Engineering 2019;141:36–41.
[14] Forsberg C, Brick S, Haratyk G. Coupling heat storage to nuclear reactors for variable electricity output with baseload reactor operation. Electr J 2018;31:23–31.
[15] Carlson F, Davidson JH. On the use of thermal energy storage for flexible baseload power plants: Thermodynamic analysis of options for a nuclear rankine cycle. J Heat Transf 2020;142:052904.
[16] Carlson F, Davidson JH. Parametric study of thermodynamic and cost performance of thermal energy storage coupled with nuclear power. Energy Convers Manag 2021;236:114054.
[17] Li Y, Cao H, Wang S, Jin Y, et al. Load shifting of nuclear power plants using cryogenic energy storage technology. Appl Energy 2014;113:1710–6.
[18] Forsberg CW. Variable and assured peak electricity production from base-load light-water reactors with heat storage and auxiliary combustible fuels. Nucl Technol 2019;205:377–96.
[19] Romanos P, Al Kindi AA, Pantaleo AM, Markides CN. Flexible nuclear power plants with thermal energy storage and secondary power cycles: Virtual power plant integration in the UK energy system. e-Prime – Adv Electr Eng Electron Energy. 2021. 2. 100027.
[20] Borowiec K, Wysocki A, Shaner S, Greenwood MS, Ellis M. Increasing revenue of nuclear power plants with thermal storage. J Energy Resour Tehcnol 2020;142:042006.
[21] Herrmann U, Kearney DW. Survey of thermal energy storage for parabolic trough power plants. J Sol Energy Eng 2002;124:145–52.
[22] International Renewable Energy Agency (IRENA). Innovation Outlook: Thermal Energy Storage. 2020.
[23] Cárdenas B, Swinfen-Styles L, Rouse J, Hoskin A, et al. Energy storage capacity vs. renewable penetration: A study for the UK. Renew. Energy 2021;171:849–67.
[24] Gils HC, Scholz Y, Pregger T, Luca de Tena D, Heide D. Integrated modelling of variable renewable energy-based power supply in Europe. Energy 2017;123:173–88.
[25] Ma Z, Davenport P, Zhang R. Design analysis of a particle-based thermal energy storage system for concentrating solar power or grid energy storage. J Energy Storage 2020;29:101382.
[26] Strbac G, Pudjianto D, Aunedi M, Djapic P, et al. Role and value of flexibility in facilitating cost-effective energy system decarbonisation. Prog Energy 2020;2:042001.
[27] Aunedi M, Wills K, Green T, Strbac G. Net-zero GB electricity: cost-optimal generation and storage mix. Energy Futures Lab White Paper 2021, https://www.imperial.ac.uk/energy-futures-lab/reports/white-papers/net-zero-gb-electricity/ [accessed 6 July 2021].
[28] Hast A, Rinne S, Syri S, Kiviluoma J. The role of heat storages in facilitating the adaptation of district heating systems to large amount of variable renewable electricity. Energy 2017;137:775–88.
[29] Aunedi M, Pantaleo AM, Kuriyan K, Strbac G, Shah N. Modelling of national and local interactions between heat and electricity networks in low-carbon energy systems. Appl Energy 2020;276:115522.
[30] Pudjianto D, Aunedi M, Djapic P, Strbac G. Whole-system assessment of value of energy storage in low-carbon electricity systems. IEEE Trans Smart Grid 2014;5(2):1098–109.
[31] Strbac G, Aunedi M, Konstantelos I, Moreira R, et al. Opportunities for energy storage: Assessing whole-system economic benefits of energy storage in future electricity systems. IEEE Power Energy Mag 2017;15:32–41.
[32] Teng F, Pudjianto D, Aunedi M, Strbac G. Assessment of future whole-system value of large-scale pumped storage plants in Europe. Energies 2018;11:246.
[33] Georgiou S, Aunedi M, Strbac G, Markides CN. On the value of liquid-air and pumped-thermal electricity storage systems in low-carbon electricity systems. Energy 2020;193:116680.
[34] International Atomic Energy Agency (IAEA). Country Statistics, Hinkley Point C-1, 2021, https://pris.iaea.org/PRIS/CountryStatistics/ReactorDetails.aspx?current=1072 [accessed 27 March 2021].
[35] EDF Energy. Nuclear New Build Projects, 2021, https://www.edfenergy.com/energy/nuclear-new-build-projects [accessed 27 March 2021].
[36] AREVA Nuclear Power and Electric de France Energy (EDF). UK-EPR, Fundamental Safety Overview, Chapter A: EPR Design Description. 2007.
[37] AREVA. European Pressurised Reactor, 2005, http://www.ftj.agh.edu.pl/~cetnar/epr/EPR-broszura.pdf [accessed 27 March 2021].
[38] Fröhling W, Unger HM, Dong Y. Thermodynamic assessment of plant efficiencies for HTR power conversion systems. International Atomic Energy Agency (IAEA) 2002.
[39] Wibisono AF, Shwageraus E. Thermodynamic performance of pressurized water reactor power conversion cycle combined with fossil-fuel superheater. Energy 2016;117:190–7.
[40] Lemmon EW, Bell IH, Huber ML, McLinden MO. NIST Standard Reference Database 23: Reference Fluid Thermodynamic and Transport Properties-REFPROP, Version 10.0. National Institute of Standards and Technology 2018.
[41] Grote W. Ein Beitrag zur modellbasierten regelung von entnahmedampfturbinen. Ph.D. Dissertation, Ruhr-Universität, Bochum,Germany. 2009.
[42] Gundogdu B, Nejad S, Gladwin DT, Foster DA. A battery energy management strategy for U.K. enhanced frequency response and triad avoidance. IEEE 26th International Symposium on Industrial Electronics (ISIE). 2017. 26–31.
[43] Cooke DH. On prediction of off-design multistage turbine pressures by Stodola's ellipse. J Eng Gas Turbines Power 1984;107:596–606.
[44] Fuls WF. Enhancement to the traditional Ellipse Law for more accurate modeling of a turbine with a finite number of stages. J Eng Gas Turbines Power 2017;139:112603.
[45] Lloyd CA, Roulstone ARM, Middleton C. The impact of modularisation strategies on small modular reactor cost. Proceedings of the 2018 International Congress on Advances in Nuclear Power Plants (ICAPP). 2018. 1042–1049.
[46] Dirker J, Juggurnath D, Kaya A, Osowade EA, et al. Thermal energy processes in direct steam generation solar systems: Boiling, condensation and energy storage – A review. Front Energy Res 2019;6:147.
[47] Xu B, Li P, Chan C. Application of phase change materials for thermal energy storage in concentrated solar thermal power plants: A review to recent developments. Appl Energy 2015;160:286–307.
[48] Wei G, Wang G, Xu C, Ju X, et al. Selection principles and thermophysical properties of high temperature phase change materials for thermal energy storage: A review. Renew Sustain Energy Rev 2018;81:1771–86.
[49] Fernández AG, Galleguillos H, Fuentealba E, Pérez FJ. Thermal characterization of HITEC molten salt for energy storage in solar linear concentrated technology. J Therm Anal Calorim 2015;122:3–9.
[50] Sarbu I, Dorca A. Review on heat transfer analysis in thermal energy storage using latent heat storage systems and phase change materials. Int J Energy Res 2019;43:29–64.
[51] Li Z, Lu Y, Huang R, Chang J, et al. Applications and technological challenges for heat recovery, storage and utilisation with latent thermal energy storage. Appl Energy 2021;283:116277.
[52] Bauer T, Steinmann W, Laing D, Tamme R. Thermal energy storage materials and systems. Annu Rev Heat Transf 2012;15:131–77.
[53] Jankowski NR, McCluskey FP. A review of phase change materials for vehicle component thermal buffering. Appl Energy 2014;113:1525–61.
[54] Liu F, Gao B, Wang S, Wang Z, Shi Z. Measurement and estimation for density of $NaNO_2$-KNO_3-$NaNO_3$ ternary molten salts. World Non-Grid-Connected Wind Power and Energy Conference (WNWEC). 2009. 1–4.
[55] Niyas H, Rao CRC, Muthukumar P. Performance investigation of a lab-scale latent heat storage prototype – Experimental results. Sol Energy 2017;155:971–84.

[56] Xiao X, Wen D. Investigation on thermo-physical properties of molten salt enhanced with nanoparticle and copper foam. 7th International Conference of Renewable Energy Research and Applications (ICRERA). 2018. 1445–1449.
[57] HITEC® Heat Transfer Salt, Coastal Chemical Co., L.L.C, Brenntag Company, Houston, Texas, United States, http://stoppingclimatechange.com/MSR%20-%20HITEC%20Heat%20Transfer%20Salt.pdf [accessed 10 November 2021].
[58] Gasanaliev AM, Gamataeva BY. Heat-accumulation properties of melts. Russ Chem Rev. 200. 69(2). 179–186.
[59] Kenisarin MM. High-temperature phase change materials for thermal energy storage. Renew Sustain Energy Rev 2010;14:955–70.
[60] Li P, Van Lew J, Chan C, Karaki W, et al. Similarity and generalized analysis of efficiencies of thermal energy storage systems. Renew Energy 2012;39:388–402.
[61] Fico Xpress Optimization, https://www.fico.com/en/products/fico-xpress-optimization [accessed 14 May 2021].
[62] Breeze P. Power Generation Technologies. Second edition. London: Newnes; 2019.
[63] Sarbu I, Sebarchievici C. A Comprehensive review of thermal energy storage. Sustainability 2018;10(1):191.
[64] National Renewable Energy Laboratory (NREL). System Advisor Model (SAM), https://sam.nrel.gov/ [accessed 12 February 2021].